Paleoenvironmental variations inferred from a high resolution pollen record of MIS 9-10 at ancient Lake Ohrid, North Macedonia

Master Thesis project Earth, Life and Climate

Yord Yedema

Supervised by Timme Donders

Utrecht University

Paleoenvironmental variations inferred from a high resolution pollen record of MIS 9-10 at ancient Lake Ohrid, North Macedonia

Yord Yedema, 4138066
Master thesis 2019
Supervised by dr. Timme Donders

Abstract

As most of central Europe suffered a successive loss of tree species during glacial-interglacial cycles, some locations in the Mediterranean acted as refugia for tree diversity for much of the Quaternary. In this thesis, I present a high resolution pollen record for Marine Isotope Stages (MIS) 9-10 (297-370 ka) from Lake Ohrid, located on the border of North Macedonia and Albania. Lake Ohrid is characterized by a high floral biodiversity throughout the Quaternary and likely acted as glacial refugium. This makes the dynamics of vegetation changes in this area interesting for research, since it presents the opportunity to study these changes in a long continuous record.

The high resolution record makes it possible to interpret short-term climate oscillations, which were mainly present between 310-297 ka. The pollen record is in good correlation with marine and terrestrial proxies, which shows that Lake Ohrid responded to both long- (glacial-interglacial) and short-scale (millennial scale) climatic fluctuations.

Furthermore, the relation between pollen production and CO_2 is investigated, by linking the pollen influx to atmospheric CO_2 concentrations, to investigate this as a potential CO_2 proxy. This showed a good overall correlation with a higher pollen influx for rising CO_2, but on shorter timescales of ~10 kyr, the trend could be different. Besides pollen production, atmospheric CO_2 levels may also have influence on carbon fractionation by plants. A new setup combining laser ablation, nano-combustion, gas chromatography and isotope ratio mass spectrometry (LA/nC/GC/IRMS) allows the measurements of carbon isotopes to single grains of *Pinus* pollen, which has been done for seven samples. The resulting $\delta^{13}C_{pollen}$ values show no trend with CO_2 levels, but interpretation of these values, using the ratio between intercellular and atmospheric CO_2 (the c_i/c_a ratio), suggest that the physiological response of vegetation to e.g. rising CO_2, is an increase in photosynthesis and a decrease in stomatal conductance. Although the c_i/c_a ratio stayed roughly constant over time, it is difficult to confidently interpret changes in c_i with changing CO_2, as it is not known if this is from c_a changes or hydrology.

1. Introduction

The understanding of environmental and ecosystem dynamics during rapid climatic changes is essential for our knowledge of current climate variations, where these changes are imminent (Fægri and Iversen, 1989; Tzedakis et al., 2009). Terrestrial climate records from glacial-interglacial periods are useful for this, as they document large variations in a range of different climate processes and as interglacial periods can present an analogue for Holocene conditions (Loutre and Berger, 2000). The study of fossil pollen is the most widely used method for terrestrial climate reconstruction and vegetation dynamics during the Quaternary, as pollen are often abundant and well preserved in for instance lake or peat sediments (e.g. Seppä, 2013).

Southern European lacustrine records are valuable for glacial-interglacial scale climate reconstruction since they show a continuous record, where glacial advances have caused unconformities in other regions. Since these regions are in close proximity of the Mediterranean Sea, marine records are also abundant from this region and present the opportunity to correlate terrestrial and marine proxy records, which is fundamental for providing a global view of climate dynamics. This relation between terrestrial and marine proxies has shown a mostly in-phase relation between North-Atlantic and Mediterranean climate variability for the Late Pleistocene, at the Iberian margin (Tzedakis et al., 2004), showing a close relation between these climate systems.

Pollens record that span multiple glacial-interglacial cycles are already available from Portugal (Roucoux et al., 2006), France (Reille et al., 2000), Greece (Wijmstra, 1969; Tzedakis et al., 1994; Tzedakis et al., 2006) and Turkey (Litt et al., 2014), but these records have a low temporal resolution of generally more than 1 kyr, which obscures possible millennial-scale climate variations. Apart from their continuous records, Southern European sites are among the best sites to study glacial-interglacial vegetation changes, as many sites act as a glacial refugium for temperate trees, where most central European locations suffered severe loss of tree species during glacial-interglacial cycles. The effect of tree migration, that often shows a lag in central and western European pollen records, is typically smaller at glacial refugia, which is favourable for linking climatic events to vegetation changes **(**Médial and Diadema, 2009**)**. To fully understand how these locations act as glacial floristic refugia, close comparison between sites is essential.

Lake Ohrid is an ancient lake located on the border of Northern Macedonia and Albania (Fig. 1), in the Southern Balkan. With a continuous sedimentary record that started between 1.2 and 1.9 Ma (Wagner et al., 2014), it is thought to be the oldest extant lake in Europe with an immense biodiversity, housing 220 aquatic species. Observed difference in climate conditions between the Central Balkans and the Lower Danube basin in the Quaternary suggest a climatic boundary, that might shield the Balkan Peninsula form harsh climate conditions from the north and allow this region to be a floristic refugium (Tzedakis et al., 2002; Obreht et al., 2016). This, plus the availability of water and its altitude causes Lake Ohrid to be a floral hotspot for temperate and montane trees and pushes its potential for paleoclimate reconstruction and research on lake evolution. In 2013, the SCOPSCO (Scientific Collaboration on Past Speciation Conditions in Lake Ohrid) drilling project was carried out within the framework of the International Continental Scientific Drilling Program (ICDP) (Wagner et al., 2014). This retrieved a continuous record showing the last ~1.5 Ma, which has been submitted to several branches of biological, geological and chemical analysis (Wagner et al., 2017). Low resolution (~1600 years) palynological research on the upper 200 m (500 kyrs) has been carried out by Sadori et al., (2016) and high resolution analysis has been done for MIS 5 and MIS 11 (Sinopoli et al., 2018; Kousis et al., 2018, respectively), as these time intervals represent some of the warmest periods of the Late Quaternary and therefore interesting subjects for climate studies.

High resolution pollen records are rather scarce in Southern Europe, leaving a gap in knowledge on the response of terrestrial ecosystems on short-term climate variability. A higher resolution allows the investigation of millennial-scale climate oscillations and provides more insight in rapid vegetation changes. For example, Kousis et al., (2018) reported several millennial scale forest contractions in their record, which they could couple to similar events at the Iberian margin, increasing the accuracy of correlations between sites and adding valuable information to the low resolution record. This added valuable information to the Lake Ohrid

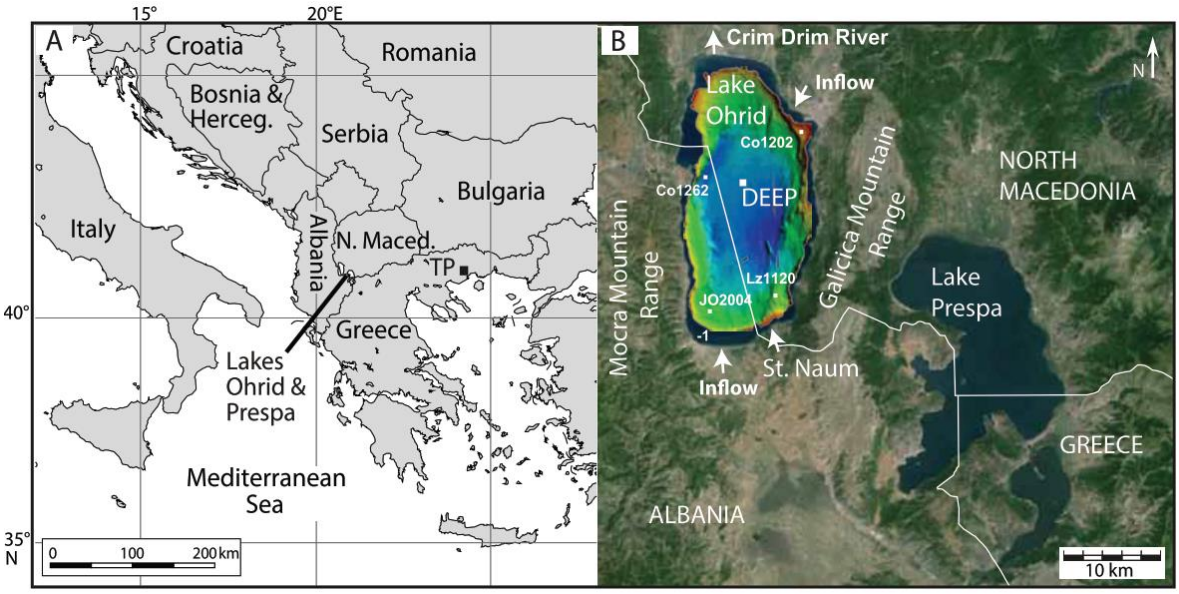

Figure 1: **(a)** Location of Lake Ohrid, adapted from Francke et al., (2016). The nearby coring location of Tenaghi Philippon (TP) in Northern Greece is also indicated.**(b)** Map of Lake Ohrid and Lake Prespa, with the Ohrid DEEP coring location.

record and demonstrated the necessity of high resolution records. To see how temperate, mesophilic and montane trees have changed with glacial-interglacial variability on millennial time scales and to see what the role of Lake Ohrid as glacial refugium is, I am increasing the resolution of the pollen record from Sadori et al., (2016), for the period between 370-297 ka (MIS 10-9), as the pollen diagram of Sadori et al., (2016) showed some climate fluctuations and interesting aspects this interval, such as a high amount of pioneer taxa. This made this interval susceptible for further, high resolution research, to investigate if these changes persisted over longer timescales or were short-lived, millennial scale events.

This pollen record can be compared to independent proxy records such as oxygen isotopes of marine deposits and speleothem records, which contributes in the understanding on glacial-interglacial climate dynamics and vegetation changes.

MIS 9-10 covers a full glacial-interglacial cycle, for which no Mediterranean high resolution pollen record is available, although records from Fletcher et al., (2013) and Kousis et al., (2018) do cover a small part of this interval.

MIS 9 is an interesting time period to investigate, as it resembles the Holocene period and the wildly studied MIS 5e (Regattieri et al., 2018; Sinopoli et al., 2018). In terms of caloric summer half-year insolation (i.e. the 182 days of the year that receive more insolation than the other 182 days, Milankovitch, (1941)), the early part of MIS 9 is the closest analogue for the Holocene of the last 450 kyr (Ruddiman, 2007). This part also experienced the highest atmospheric CO_2 concentrations before the industrialisation (close to 300 ppm, Bazin et al., 2013), the highest Antarctic temperatures (Petit et al., 1999) and modern day sea levels (Rohling et al., 2009). After the early part of MIS 9, CO_2 concentrations and temperatures gradually decreased and ice volume increased. Other Southern European pollen records show increased variability after MIS 9e (Reille et al., 2000; Roucoux et al., 2006; Fletcher et al., 2013). Deciduous oaks and montane trees are the main constituents of forests during this interval, which are also dominated by pine trees. MIS 10 was characterized by cold conditions. Glacial expanses were present, but not as severe as for example the later MIS 6. Sea level was 100 meters lower than today (Rohling et al., 2009) and atmospheric CO_2 concentrations were below

200 ppm (Lüthi et al., 2008). Other pollen records from this interval show a vegetation dominated by grasslands (e.g. Roucoux et al., 2006; Litt et al., 2014). Another interesting aspect of MIS 9 and 10 is the disappearance of some currently relict taxa at the nearby sites of Tenaghi Philippon and Ioannina (Magri et al., 2017), such as the European pecan (*Carya*), the wingnut (*Pterocarya*) and *Zelkova*, from the elm family. These disappearances are related to climatic variability, but the exact timing of these events is still unknown in this region. As Lake Ohrid is also located in the Balkan Peninsula, it can act as a supplement to this database of relict taxa. Comparing the pollen record to marine proxies from the Mediterranean region puts the Lake Ohrid record in a broader context and allows a better age constraint by linking similar events to each other. To correlate the terrestrial pollen record to marine proxies, it is beneficial to link the pollen record to Marine Isotope Stages and substages. This is achieved by dividing the pollen record into distinct zones, which can be correlated to MIS substages. The transitions of Marine Isotope Stages and the usage of substages has, however, been performed inconsistently. Railsback et al., (2015) have proposed to define a scheme for the last million years, based on the benthic isotope stack of LR04 (Lisiecki and Raymo, 2005). For MIS 9, five substages are defined by Tzedakis et al., (1997), lettered a-e. MIS 10 has three substages, a-c, first defined by Lundberg and McFarlane (2007). This scheme is used in many studies (e.g. Fletcher et al., 2013; Sadori et al., 2016; Regattieri et al., 2018) and the same amount of substages will be implemented here. The exact position of these transitions is investigated with the pollen record, mainly based on the percentages of AP-*Pinus* pollen.

Another interesting aspect in the pollen record of Sadori et al., (2016), is the resemblance of pollen concentration and benthic isotope stacks. The benthic isotope stack represents a glacial-interglacial ice volume, which possibly represents CO_2 levels. An increase in atmospheric CO_2 and temperature leads to long term population increase and short-term plant growth due to higher rates of photosynthesis, leaf duration and growth area on leaves, while also extending the growing season (Ceulemans and Mousseau, 1994). This relationship is complex, as water and nutrient availability play a crucial role in plant growth. Rises in biomass around the lake can then be explained by higher temperatures or CO_2 levels. To increase our understanding of the relation between pollen production and atmospheric CO_2, pollen accumulation rates will be linked to paleo-CO_2 levels, by calculating the pollen influx. Based on this correlation, the potential of pollen production as atmospheric CO_2 proxy can be investigated.

Experiments with pollen production under elevated CO_2 concentrations by LaDeau and Clark (2006) on *Pinus taeda* showed interesting results. They showed that trees growing under elevated CO_2 concentrations (+ 200 µL/l CO_2) started producing pollen at a younger and smaller state than trees growing in normal conditions, based on their diameter. The amount of pollen produced did not significantly change, as was evident from experiments with air samples (LaDeau and Clark, 2006). Since most temperate tree taxa are wind-pollinated (Burns and Honkala, 1990), their dispersal is controlled by wind accessibility. Trees in short, dense canopies have less access to wind and will disperse more locally. This causes the ecological effect of elevated CO_2 levels on pollen production to be quite low (Farris and Mitton, 1984). This could be a local effect, as a long-term CO_2 increase does have ecological consequences as a rise pollen production. Other studies using ragweed (*Ambrosia artemisiifolia*) showed a relatively linear increase in pollen production with high CO_2 (Ziska and Caulfield, 2000).

An increase in pollen production by increasing CO_2 is an interesting research subject in climate change studies, as this is in present days troublesome for people with pollen allergies. In the Mediterranean area, a rise in CO_2 will likely increase the pollen production, but will not change the vegetation that much, as this has to be paired with a reduction in precipitation of

30%, similar to the modern day conditions of the southern Mediterranean (Cheddadi et al., 2001).

Besides the effect of changing CO_2 levels on the production of pollen, it can also have an effect on the isotopic composition of pollen. Variations in carbon fractionations can be the result of carbon limitation during glacial-interglacial cycles. These carbon fractionations can be used to unravel the physiological response of vegetation to changes in atmospheric CO_2 and humidity. This effect will be investigated by measuring the carbon isotope signature of pollen grains, with a new instrumental method that has recently been installed at Utrecht University (van Roij et al., 2017). Here, laser ablation is combined to nano-combustion, gas chromatography and isotope ratio mass spectrometry (LA/nC/GC/IRMS). This technique allows analysis on smaller samples, as similar analyses were limited to at least several µg of carbon (e.g. Moran et al., 2011; Nelson, 2012). The increase in analytical window/detection level opens the door for palynological analysis on microfossils, as has been tested for dinoflagellates. Applied to pollen, this greatly enhances the geological timescale in which the fractional carbon uptake of plant material can be studied, as the sporopollenin in pollen is extremely resistant to degradation and allows pollen to remain in the sedimentological record for much longer than other plant material.

To test pollen grains as a potential paleo CO_2 proxy and the applicability of this setup on pollen, several samples have been selected for carbon isotope analysis. The main question that arises here, is if this isotope signature reflects changes in the atmospheric CO_2, precipitation, or displays changes in the plants internal biochemistry, which will be investigated using the c_i/c_a ratio (Farqurah et al., 1982), which is the ratio between intercellular and atmospheric CO_2. This can provide additional information on vegetation dynamics around Lake Ohrid.

2. Site Setting

Lake Ohrid (40º54’ to 41º10’ N, 20º38’ to 20º48’ E, 693 m a.s.l.), is located at the southern Balkan Peninsula on the border of Northern Macedonia and Albania (Fig. 1). It is situated within the Dinarides-Albanides-Hellenides mountain range, which formed at the final phase of Alpine orogenesis. It lies in a N-S-trending tectonic graben that has formed between 2-10 Ma (Lindhorst et al., 2015), while the onset of lake formation is estimated to be 1.5-3 Ma (Wagner et al., 2014). The lake is tub-shaped, has a maximum length of 30.8 km, a maximum width of 14.8 km, a surface area of 358 km^2 and an average and maximum water depth of 150 m and 293 m, respectively (Lindhorst et al., 2015; Popovska and Bonacci, 2007).

The catchment area is 2600 km^2, where most inflow comes from direct precipitation (25%), riverine inflow (25%) and karst aquifers (50%). This is balanced by evaporation (40%) and riverine outflow of the Crni Drim river in the northern part of the lake (60%) (Matzinger et al., 2006). Based on the ratio between water volume and outflow, the hydraulic residence time is approximately 70 years, with a complete overturn every 7 years (Matzinger et al., 2006), although this can be influenced by incomplete mixing.

Lake Ohrid is connected through underground karst channels with sister lake Prespa, located 10 km to the east and is separated from lake Ohrid by the Galičica mountains (2265 m a.s.l.). Although connected, Lake Ohrid and Prespa react differently to external forcing, based on diatom data (Cvetkoska et al., 2015), as Lake Prespa is also more susceptible to eutrophication, since its much shallower than lake Ohrid and thus has a smaller water volume (Albreth and Wilke, 2008; Matzinger et al., 2007). Due to their underground connection, it is difficult to

determine their separate spatial distribution (Watzin et al., 2002; Popovska and Bonacci, 2007). Their combined catchment area would be 3921 km^2.

Apart from the Galičica mountains, other mountain ranges also surround the lake and can be found in the southeast (Mali I Thatë mountains, 2028 m a.s.l.), the west (Mokra mountains, 1514 m a.s.l.) and the northwest (Jablanica mountains, 1945 m a.s.l.). Devonian siliciclastic bedrock, intensely karstified Triassic limestones and ultramafic metamorphic and magmatic rocks from the Jurassic and Cretaceous dominate the eastern and western shore of the lake (Hoffman et al., 2012). The plains in the northern and southern shore are covered with Quaternary deposits.

Local climate

The local climate belongs to the Mediterranean regime, with generally warm and dry summers and cold and wet winters. Due to the altitude and distance from the Adriatic Sea, Lake Ohrid is also under influence of a continental climate (Watzin et al., 2002). During winters, moisture availability is controlled by the southward migration of the Intertropical Convergence Zone, allowing westerlies to track over the Mediterranean region, and by convective precipitation. Cold conditions are related to southward expansions of polar air masses from the Siberian High (Saaroni et al., 1996), while hot and dry summer conditions are linked to expansions of the Azores High (Xopakli et al., 2003). Main wind directions are north-south and are controlled by the basin morphology (Stanković, 1960).

Annual temperatures range from -5.7 ºC to 31.5 ºC, with an average temperature of 11.1 ºC, while the average annual precipitation is around 900 mm (Popovska and Bonacci, 2007).

Modern vegetation

Lake Ohrid has a rich diversity of local flora, which is mainly dominated by Mediterranean and Balkan elements, as well as several central European taxa (Matevski et al., 2011). The catchment vegetation is organized in altitudinal belts, from the lake level at 693 m a.s.l. to the top of the mountains at 2200 m a.s.l. Grasslands and agricultural fields are found in the lowlands surrounding the lake, together with riparian forests dominated by *Salix alba.* Close to the lake, forests consists mostly of mixed deciduous and semi-deciduous taxa (e.g. *Quercus cerris*) and hornbeams (*Carpinus orientalis, Ostrya carpinifolia*), followed up by mesophilous and montane taxa such as beeches, hornbeams, hazels and maples(*Fagus sylvatica, Carpinus betulus, Corylus colurna, Acer obtusatum).* Firs (*Abies alba, A. borisii-regis*) form the upper part of the forested area. Above the timberline, at 1900 m a.s.l. (Matevski et al., 2011), alpine grasslands and *Juniperus* shrubs, together with sparse populations of Macedonian and Bosnian pine (*Pinus peuce, P.heldreichii*), which are considered Tertiary relics. The presence of glaciers on top of the Galičica mountains is documented for glacial periods, that did not reach the lake shore (Ribolini et al., 2011).

Lake Ohrid itself is known for its rich local macrophytic flora, which is dominated by *Lemna triscula, Myriophyllum-, Potamogeton-* and *Chara* species (Albreht and Wilke, 2008).

3. Methods

The pollen samples are retrieved from the DEEP site in the middle of Lake Ohrid (Fig. 1). A total of 1526 m has been recovered, using five boreholes and comprising a 569 m continuous record. The age model is based on eleven tephra layers from Italian eruptions. Second-order tie points correlate Total Inorganic Carbon (TIC) to orbital forcing and the age model was

eventually cross-evaluated with the bore logging data from Baumgarten et al., (2015). Three distinguishable lithotypes have been identified in the lake. Lithotype 1 and 2 comprise of calcareous and slightly calcareous siliciclastics, respectively, while lithotype 3 consists of clastic material (Francke et al., 2016). Lithotype 1 and 2 are mostly present during interglacial intervals, while lithotype 3 is mostly present during glacial intervals. Additional information about the SCOPSCO core retrieving and sub-sampling can be found in Wagner et al., (2014) and Francke et al., (2016).

Sub-samples were taken of every 16 cm, which corresponds to ca. 400 years (Francke et al., 2016). For the upper 200 m, pollen analysis has been carried out with a resolution of 64 cm (~ 1600 years), corresponding to the last 500 kyrs (Sadori et al., 2016; Bertini et al., 2016).

Pollen analysis

A total of 43 samples taken between 129-157 m.b.l.f. have been prepared for taxonomical analysis. These samples have been taken at a 64 cm interval, in between the samples already analysed by Sadori et al., (2016), resulting in a combined resolution of 32 cm. Using the updated age model (Wagner et al., accepted), the samples have a resolution of ~600 to 1000 years.
The samples have been prepared via the Rome protocol, which is the procedure used for Lake Ohrid preparations (slightly modified from Faegri & Iversen, 1989; Sadori et al., 2016). First, the samples are freeze dried and weighted afterwards in plastic tubes, so that around 1 gram of material per sample is used. Two tablets of 9666 *Lycopodium* spores are added per sample to make an estimation for the pollen concentration (Stockmarr, 1971). 30% HCl is added to dissolve the *Lycopodium* tablets and to remove the carbonates. After each step, every tube has been centrifuged and decanted carefully, to prevent loss of sample. For the silicate removal, HF (40%) was used by shaking the samples for two hours and leaving them overnight. After HF treatment, the samples were decanted again and treated with HCl to remove fluoride gels.
KOH (10%) was added to discard organics out of the sample. This should leave a yellowish colour after centrifuging the samples. Afterwards, water is appended to the samples to clean them from the KOH. Since sporopollenin is a highly resistant substance, it is not significantly affected by these acids.

Fine sieving is done with a 125 µm and a 7µm sieve and by holding the sieves in an ultrasonic bath, so that mostly pollen material stays behind. For the slide preparation, ethanol was added to the sample, to remove possible salt remains and dewater the sample. A few drops of glycerol was added for the slide preparation. Per sample, two slides were made, using the glycerol mounting technique, allowing pollen to move around when pushing the slide with a small wooden stick. The residue is preserved for further analysis on the carbon isotopes.

The slides were analysed with a Leica photo microscope equipped with differential interference contrast (DIC). At least 300 pollen were counted per sample, excluding *Pinus* due to its overrepresentation. Reported *Pinus* percentages are based on a sum which includes *Pinus*. Oak pollen were divided into three groups according to Smit (1973); *Quercus robur*, which includes deciduous oaks, *Quercus ilex*, including Mediterranean (evergreen) oaks – *Q. suber* and *Quercus cerris*, including semi-deciduous oaks and *Q. suber*. *Juniperus* type contains *Cupressus*, *Juniperus* and *Taxus*. *Pinus* has been divided into diploxylon and haploxylon subgenera (Appendix 1). This division shows differences in their phenolic patterns, i.e. if they have two or one fibrovascular bundle per leaf, respectively, (Koehne, 1893). Identification has been done by using the key of Beug (1961) and Moore et al., (1991). Pollen diagrams have been made using C2 software (Juggins, 2003). Pollen zones are defined with CONISS (Grimm, 1987)

and follows the approach by Sinopoli et al., (2018), based on the Pollen Super Assemblage Zones (PASZ) as defined by Sadori et al., (2016).

Paleo-CO_2 correlations and carbon isotope analysis:

To test the relation of pollen production to atmospheric CO_2, an estimate for the total pollen concentration is needed. This is done by counting the amount of Lycopodium spores in a sample. Since the number of Lycopodium spores in a sample is known, the counted Lycopodia can be extrapolated to the total pollen grains in a sample. Combined with the weight of the sample, the concentration can be calculated. This is then converted to pollen influx, i.e. the pollen concentration multiplied with the sedimentation rate, which is a more practical term in ecology. Pollen influx is estimated in grains/cm^2/ year. The sedimentation rate is here calculated by dividing the depth by the age of a sample. Lindhorst et al., (2015) found an average sedimentation rate of 0.41 mm a year, for the last 430 kyr for Lake Ohrid, which does agree with the data calculated here. The pollen production of different pollen groups are investigated, with a main focus on tree pollen. For paleo-CO_2 data, ice cores from EPICA are used (Bereiter et al., 2015).

To test the instrumental setup of van Roij et al., (2017) on pollen grains, seven pilot samples have been chosen throughout the studied interval to measure the $\delta^{13}C$ of these pollen. This includes two samples on opposing ends of a major vegetation transition and atmospheric CO_2 gradient, allowing insight on the effect of rapid changing climates on the internal carbon response mechanisms in plants. *Pinus* grains were chosen due to their overrepresentation in most samples and because their size (>50 µm) allows measurements on single grains. For two samples where these taxa were abundantly present, pilot measurements have also been made on *Quercus robur* and *Abies,* to test this instrumental technique for a variety of different pollen grains.

The residues were sieved again with ultraclean water, to rinse out the glycerine that was used to prepare the slides. For the whole preparation process, ultraclean water is used as this minimizes changes of contamination. After rinsing, parts of the residue is put in a small glass container in a drop of ultraclean water, and were examined under an compound light microscope, that illuminated the sample from below. Per sample, around 120 *Pinus* grains were picked and isolated by hydraulic suction using a specialized pipet, connected to a small cable supplying ultraclean water to the pipet. By manually altering this water supply, pollen grains can be picked out of the residue, by sucking up the pollen grains and spilling them out again in a separate drop of water. This is done multiple times to ensure that only *Pinus* grains are isolated. The pollen grains are subsequently placed in the middle of a small nickel disc (diameter ~6 mm), in a small drop of water. As this water droplet evaporated, the pollen grains were repositioned under a binocular towards the middle of this nickel disc, since the laser does not reach the outer edges of the disc, causing loss of sample. The pollen grains were hydraulically pressed by placing another nickel plate on top of the samples, to adhere the grains to the surface of the plates. The two plates are separated again, where ideally the majority of the pollen stick to one of the two plates.

A small piece of IAEA CH-7 polyethylene (PE) was placed next to the grains to act as the standard for $\delta^{13}C$ (van Roij et.al., 2017). This foil has a known $\delta^{13}C$ value of -32.151 +- 0.050 and is used to correct the measurements (Coplen et.al., 2006). One of these plates is put in the ablation chamber from below, which is connected to two suction pumps that maintain a vacuum in the ablation chamber, so that no leakage from atmospheric gasses into the system occurs (van Roij et al., 2017). The ablation chamber is put under the microscope where it is exposed to a

laser that shoots the material for several seconds with on average 45 mJ, compared to 100 mJ for the standard. Samples are measured in the combustion oven, which is connected with the ablation chamber through spooling wires, which maintain a continuous helium flow. Per run, five PEs and six grains are measured, which, with six runs per sample, would result in a maximum of 36 measurements. Between every measurement, there is a waiting time of approximately five minutes, as the $\delta^{13}C$ must be reduced to background levels. If the next measurement is done too fast after the previous one, the baseline of the peak is elevated, which results in wrong values. For these measurements, only 36 *Pinus* grains are needed, but loss of sample can occur during many steps of the preparation process, for instance by pollen grains that stick to other organic material and is subsequently ignored to avoid contamination, sticking to the inside of the pipet, sticking to the other nickel plate that is used to flatten the pollen and by pollen being located too close to the edge of the nickel plate. Therefore, it is recommended to pick a large amount to account for this and to concentrate them in the middle of the nickel plate before hydraulically pressing them. This can be a challenging task when dealing with smaller pollen grains, as for example *Q. robur* pollen are smaller and thus a larger amount of pollen grains is needed, since their size is unfit for single grain analysis. Up to 200 *Q. robur* pollen grains have been picked to try to account for this.

According to van Roij et al., (2017), samples up to 13 ng C (0.85 Vs) have a precision of 1.74‰, while samples down to 24 ng C (2.06 Vs) have a precision of 1‰. *Pinus* grains generally had a peak of around 0.7 Vs, which corresponds to 12 ng of carbon. This limits the accuracy of the measurements a bit, making it harder to interpret variability of the measurements as natural variation or analytical variation.

Integration is done with Isodat 3.0 software (Thermo Fischer), where the data is checked on elevated baselines and the size of the peaks, before being corrected for the PE. The measurements per sample are averaged, so that every sample has its own $\delta^{13}C$ signature.

4. Results

Vegetational changes at Lake Ohrid

The palynological samples showed a wide variety of taxa, with generally 35-45 different taxa per sample and around 140 different taxa in total. In samples dominated by tree pollen (arboreal pollen, AP), a high pollen concentration was present, with generally over 50.000 grains/gram to over 300.000 grains /gram, while lower concentrations (1.000-15.000 grains/gram) were found in herb dominated samples (non-arboreal pollen, NAP) (Appendix 2 and 3). The mean count was 632 pollen per sample (*Pinus* included). Pollen that were severely reworked or folded in a way that recognition would be an estimate, are labelled as undeterminable. This groups generally consists of less than 10% per sample, but is still significantly higher than in the previously counted samples by Sadori et al., (2016).

Pollen diagrams are divided into eleven pollen zones OD-10 – OD-8F (Fig. 2 and Fig. 3, Table 1), consistent with previously defined super zones at Ohrid DEEP (Sadori et al., 2016). Small offsets between the pollen zones and MIS boundaries as defined by Railsback et al., (2015) can occur due to uncertainties in the age model, which is less well constrained for MIS 9-10 due to the absence of tephra layers in this interval (Francke et al., 2016).

In general, steppe vegetation consisting of mostly *Artemisia, Chenopodicaceae* and *Poaceae* was present during glacial intervals, while the interglacial of MIS 9 shows a wide range of mesophilous and montane forests, with also riparian and Mediterranean elements. *Pinus* is high in abundance during the whole interval, with a clear dominance of the diploxylon subgenera

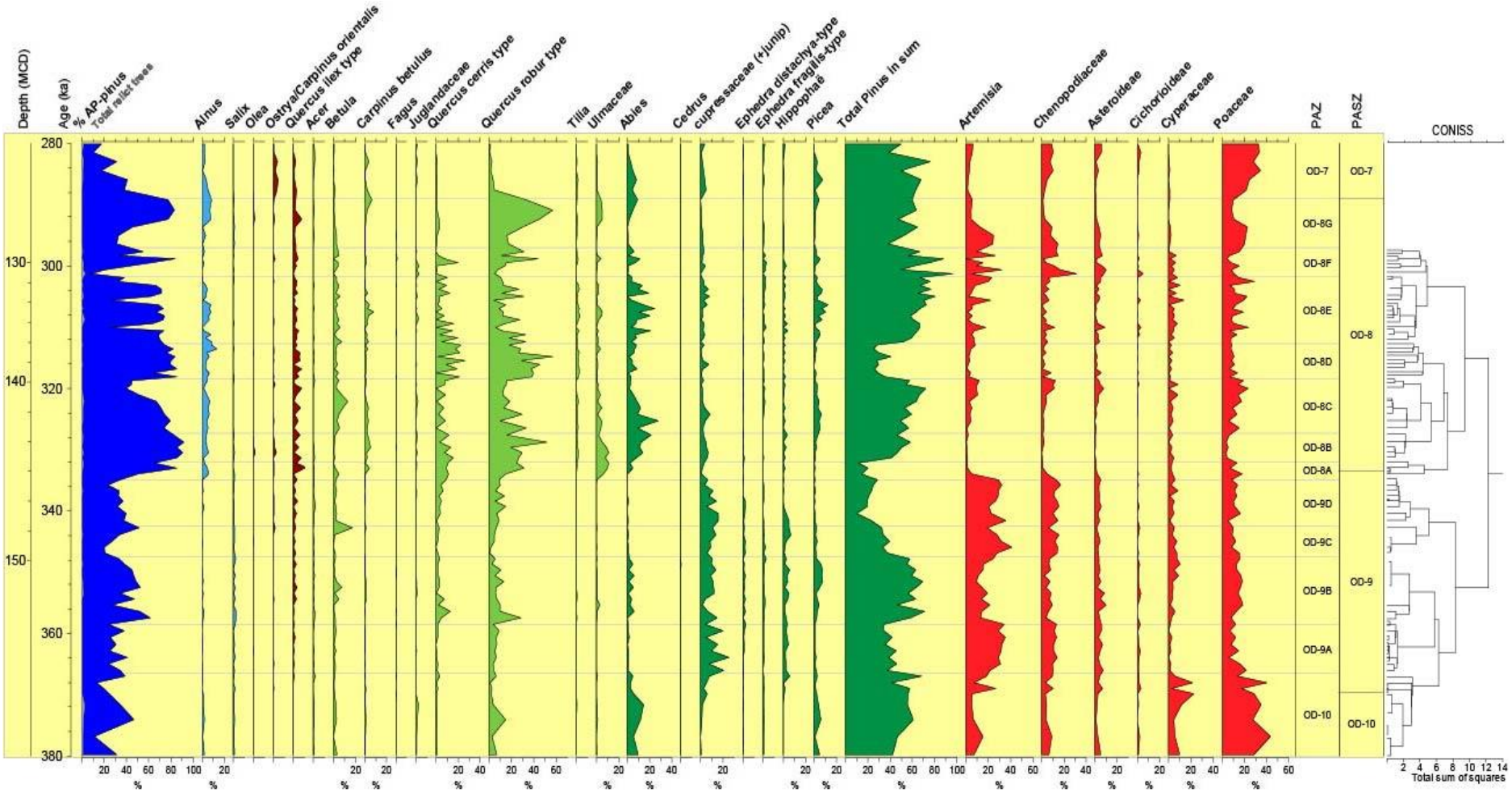

Figure 2: Lake Ohrid (North Macedonia, Albania) DEEP core – Pollen percentage diagram (selected taxa) against depth and age. Colours indicate ecological groups and are described in Fig. 3. The pollen zones are defined by using CONISS. Pollen Assemblage Zones (PAZ) are listed in Table 1.

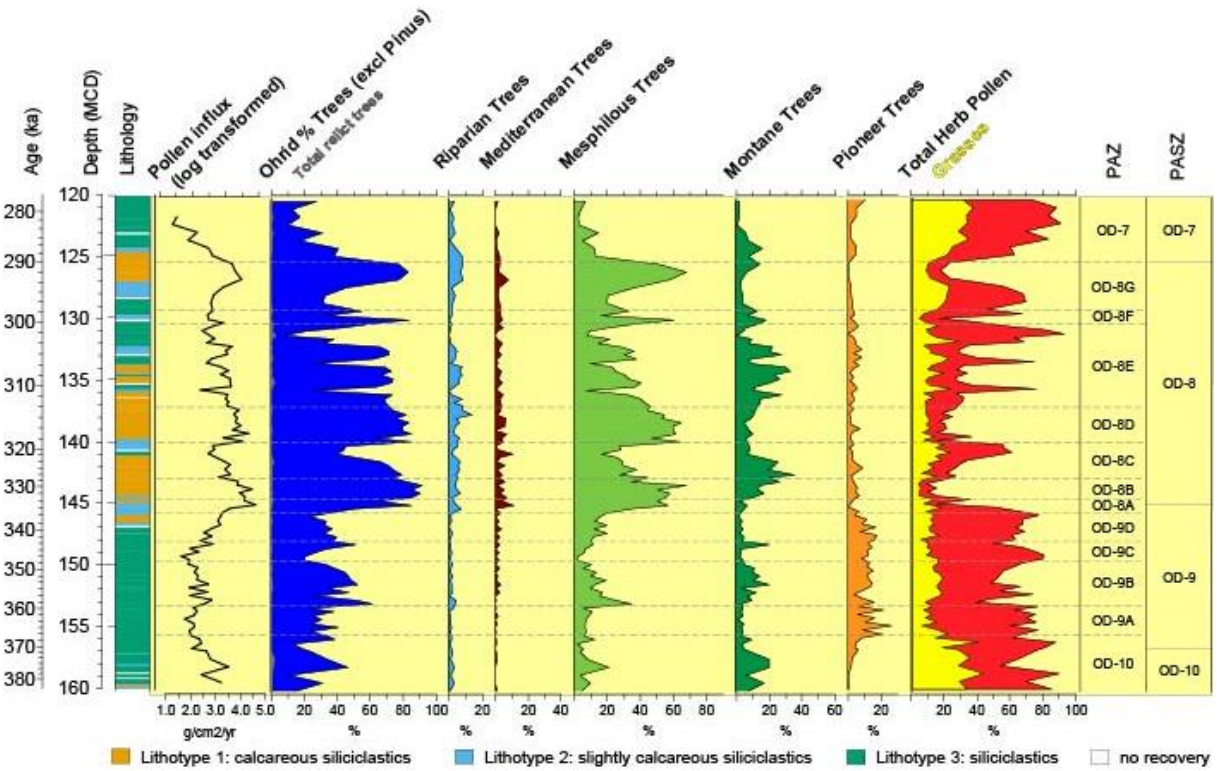

Figure 3: Lake Ohrid (North Macedonia, Albania) DEEP core – Pollen diagrams of selected ecological groups (%) and pollen influx against depth (m), age (ka), and lithology (Francke et al., 2016). The log transformed pollen influx is calculated by multiplying the pollen concentration with the sedimentation rate. Riparian trees (*Alnus, Platanus, Populus, Salix, Tamarix*), Mediterranean trees (*Arbutus, Cistus, Fraxinus ornus, Olea, Phillyrea, Pistacia, Quercus ilex, Rhamnus*), mesophilous trees (*Acer, Aesculus, Buxus, Carpinus, Castanea, Carya, Celtis, Corylus, Fraxinus excelsior, Hedera, Ostrya, Pterocarya, Quercus cerris, Q. robur, Tilia, Tsuga, Ulmus, Zelkova*), montane trees (*Abies, Betula, Fagus, Ilex, Picea, Taxus*), pioneer trees (*Cuppressaceae, Ephedra distachya, E. fragilis, Ericaceae, Hippophaë, Juniperus, Taxus*). Total herbs covers all non-arboreal pollen, excluding *Poaceae*, which is plotted under grasses. Relict taxa (*Carya, Cathaya, Cedrus, Engelhardia, Eucommia, Liquidambar, Pterocarya, Sciadopitys, Sequioa, Taxodium,* Tsuga). Pollen assemblage zones are described in Table 1.

relative to the haploxylon subgenera, although its influx drops at the end of the glacial stage (Fig. 2). Several NAP taxa (i.e. *Asteroideae, Brassicaceae, Caryophyllaceae, Chichorioideae, Galium, Thalictrum)* are consistently present in the glacial period (Appendix 4).

The base of the record (pollen zone OD-10) spans from 380-366.6 ka and marks the last part of MIS 11. Grasses were most dominant during this period, where herbs like *Artemisia* and *Chenopodicaceae* were moderately present. The steppe vegetation alternates with forests consisting montane and mesophilous components (*Abies, Q. robur*), with AP percentages up to 46%.

The interval between 366.6 and 358.5 ka (OD-9A) shows the transition into the glacial period of MIS 10 and corresponds to MIS 10c. Pioneer taxa such as *Juniperus, Ephedra* and *Hippophaë* increased sharply from 1% to 20-25%, while the environment was also dominated by NAP taxa (*Artemisia, Asteroidea, Chenopodicaceae, Poaceae*). *Pinus* influxes started to decrease, while still remaining abundant (45%). AP components are low. During OD-9B (358.5-347.5 ka), a slight recovery of temperate forests is seen, with increases in AP (*Pinus, Picea, Q. robur, Abies, Salix)* and grasses, while *Artemisia* and *Chenopodicaceae* decrease, characterizing the small interstadial of MIS 10b (Railsback et al., 2015). A sudden, short-lived peak in Quercus pollen is seen at 357.7 (from 3 to 28%), indicating a period of forest expansion, although this could also be a counting artefact, as it is the only taxa showing a rapid increase in this interval.

Table 1.

Lake Ohrid (Northern Macedonia, Albania) DEEP core – Main vegetational features divided into pollen zones. PAZ indicates the Pollen Assemblage Zones.

PAZ	Age (ka) Duration (kyrs) Depth (m)	AP% AP excl. *Pinus* % Mean AP excl. *Pinus* %	Vegetation Main pollen components
OD-8F	301.8 – 297	60 – 98	Mesophilous/Steppe alternations
	4.1	7 - 83	*Pinus, Q. robur, Artemisia, Chenopodicaceae, Poaceae,*
	130.99 – 129.06	43.7	*Q. cerris*
OD-8E	312.7 – 301.8	74.8 – 93.4	Mesophilous, Montane
	10.9	24.7 – 74.2	*Pinus, Q. robur, Abies, Q. cerris, Poaceae, Cyperaceae,*
	136.75 – 130.99	60.7	*Picea*
OD-8D	318.4 – 312.7	74.5 – 90.3	Mesophilous, Riparian
	5.3	64.0 – 85.4	*Q. robur, Q. cerris, Pinus, Poaceae*
	139.63 – 136.75	78.8	
OD-8C	327.3 – 318.4	74.9 – 89.5	Montane, Mesophilous
	8.9	39.5 – 79.3	*Pinus, Poaceae, Abies, Q. robur, Artemisia,*
	142.51 – 139.63	60.5	*Chenopodicaceae, Betula*
OD-8B	332.1 – 327.3	91.2 – 96.4	Mesophilous, Montane, Mediterranean
	4.8	85.0 – 91.5	*Q. robur, Pinus, Abies, Q. cerris, Ulmaceae*
	144.43 – 142.51	86.9	
OD-8A	334.9 – 332.1	57.2 – 88.0	Mesophilous, Meditteranean
	2.8	50.0 – 84.9	*Q. robur, , Q. cerris, Poaceae, Pinus Ulmaceae, Q. ilex*
	145.39 – 144.43	66.6	
OD-9D	342.4 – 334.9	42.4 – 53.0	Steppe
	7.5	23.1 – 39.8	*Artemisia, Chenopodicaceae, Poaceae, Pinus, Juniperus*
	147.63 – 145.39	33.7	
OD-9C	347.5 – 342.4	46.6 – 67.0	Steppe
	5.1	19.9 – 51.3	*Artemisia, Pinus, Chenopodicaceae, Poaceae, Juniperus,*
	149.23 – 147.63	30.4	*Betula*
OD-9B	358.5 – 347.5	60.7 – 86.0	Steppe, Montane
	11	27.1 – 61.2	*Pinus, Artemisia, Poaceae, Juniperus, Q. robur*
	153.07 – 149.23	44.1	*Cyperaceae*
OD-9A	366.6 – 358.5	49.9 – 63.6	Steppe
	8.1	23.6 – 40.9	*Artemisia, Juniperus, Pinus, Chenopodicaceae, Poaceae,*
	155.31 – 153.07	30.2	
OD-10	380 – 366.6	49.0 – 80.6	Steppe/montane alternations
	13.4	11.3 – 46.6	*Pinus, Poaceae, Artemisia, Cyperaceae, Abies*
	161.07 – 155.31	27.3	

Forests disappeared again during OD-9C and OD-9D (347.5-342.4 ka and 342.4-334.9 ka, respectively), where glacial conditions prevailed again, with dominant steppe taxa (up to 80%). This is coupled to a steady decrease in *Pinus* influx, that reaches an absolute low of 10% during OD-9D (Fig. 2). At the end of OD-9C, an abrupt rise in *Betula* is visible, at 342.8 ka, which could also be a counting artefact. Together, both pollen zones correspond to MIS 10a, which is characterized by glacial climates.

The transition of glacial to interglacial conditions is documented in OD-8A (334.9-332.1 ka). Steppe taxa makes place for dominantly temperate forests, that includes mesophilous (*Q. robur, Q. cerris, Carpinus betulus, Tilia, Ulmus, Zelkova*) and Mediterranean taxa (mainly *Q. ilex*), as well as a rise in *Alnus*. AP-*Pinus* gradually increased from 35% at 335 ka to 85% at 333 ka, while the *Pinus* influx remains low. The following pollen zone OD-8B (332.1-327.3 ka) is also characterized by temperate forests, with the addition of montane taxa (*Abies, Picea*) and an increase in *Pinus* to 60%. AP-*Pinus* becomes most dominant of the whole interval (90%),

indicating peak interglacial conditions, corresponding to MIS 9e (Railsback et al., 2015; Lacey et al., 2016). These interglacial conditions prevail until the end of OD-8C (327.3-318.4 ka), where AP-*Pinus* drops to 45%, accompanied with a comeback of steppe taxa (321-318 ka, Fig. 2). This short interval of forest contraction is likely linked to the stadial conditions of MIS 9d. OD-8D (318.4-312.7 ka) sees the return of the temperate forests, mostly consisting of *Q. robur*, *Q. cerris* and *Abies*, but also with a decrease in *Pinus*. Riparian vegetation, mostly consisting of *Alnus*, is relatively abundant during this period. The dominance of *Pinus* in the record re-establishes in OD-8E (312.7-301.8), as forests gradually consist of more montane elements compared to mesophilous taxa. This period is characterized by two abrupt forest contractions; at 310 ka and 305.7 ka, where AP-*Pinus* drops from 70 to 25%. The interstadial period of MIS 9c is here related to the interval of 318-303 ka, where AP was abundant. A larger drop in AP-*Pinus* characterizes the start of OD-8F (301.8-297 ka), where NAP taxa become dominant again. This alternates with mesophilous forests, where deciduous oaks are the most dominant elements, showing the onset of vegetation changes indicative to cooler climate conditions, likely related to MIS 9b. The end of the interglacial, MIS 9a, is not present in this high resolution interval, but has been added to the figures to encompass the entirety of MIS 9.

Relict taxa

The timing of tree extinctions in southern Europe during the Quaternary varies immensely with location (Magri et al., 2017). MIS 9 is an interesting interval to probe the disappearance of several taxa (i.e. *Carya, Cathaya, Cedrus, Liquidambar, Pterocarya, Zelkova*) in south-eastern Europe, as is documented at Tenaghi Philippon (Wijmstra, 1969) and Ioannina (Tzedakis et al., 2001). Since Lake Ohrid is in the vicinity of these sites and acted as glacial refugium, it can add valuable information to pinpoint the disappearances of these taxa in the Balkan Peninsula. Since correct identification of these taxa is vital for making interpretations on the state as glacial refugium that Lake Ohrid has, photos of discussed taxa are shown in Appendix 1.

Cedrus, *Cathaya* and *Liquidambar* are nearly absent during MIS 9 or 10. *Cedrus* has been documented once, while *Cathaya* and *Liquidambar* were sporadically found, although mostly in the samples counted by Sadori et al., (2016). *Cedrus* reappears at Lake Ohrid during MIS 5 and even later, while *Cathaya* and *Liquidambar* have their last occurrence in MIS 9 (Donders et al., in preparation), although *Liquidambar* is currently still a relict species on Rhodos and in South-West Turkey.

Carya and *Pterocarya* are continuously present in low amounts at Lake Ohrid, showing that both taxa do not completely disappear from the site until MIS 7 (Kousis et al., 2018; Donders et al., in preparation). Similar trends are seen at Tenaghi Philippon (Tzedakis et al., 2006). In Europe, *Carya* was a dominant taxa in most forests 1.5 Ma and since the Middle Pleistocene, it follows a disappearing trend from western to eastern Europe (Magri et al., 2017). *Pterocarya* was also initially widespread in Europe and its last occurrences are documented at MIS 7 or 9, varying per site. At Lake Ohrid, being relatively abundant during MIS 11, it was present during MIS 9 and disappears during MIS 7, as it is not present in MIS 5 (Kousis et al., 2018; Sinopoli et al., 2018). *Zelkova* was more prominently present during MIS 9 (up to 6%), which is also recorded at Tenaghi Philippon (Wijmstra, 1969), while its last appearance is also later than other taxa. Although *Zelkova* is not present on continental Europe in modern times, it still can be found on the islands of Sicily and Crete. Its disappearance is linked to gradual cooling and in most sites, its last appearance correlates with the Eemian interglacial (Magri et al., 2017). At Lake Ohrid, it is of moderate abundance during MIS 9 and was also still present in MIS 5 (Sinopoli et al., 2018).

Carbon isotopes of single pollen:

To see the physiological response of plants to changing CO_2, the carbon fractionation was measured, for seven pilot samples. The mean $\delta^{13}C$ measurements of *Pinus* grains per sample are presented in Fig. 4 and Table 2. For the $\delta^{13}C$ values of individual measurements, see Appendix 5.

On first glance, no long-term trend is visible in the $\delta^{13}C$ values. Samples deviate between -27.69 and -26.48‰, expressing a more or less see-saw pattern. These values are consistent with $\delta^{13}C$ values of wood cellulose and leaf material of C3 plants growing in temperate climates (Kohn et al., 2010), although it should be noted that there can be a discrepancy between the $\delta^{13}C$ of sporopollenin and of untreated pollen (Descolas-Gros et al., 2007). The range between the samples is approximately 1.2‰, while the majority of individual measurements ranges between -31 and -24‰ (Appendix 5). Single *Pinus* grains were typically sufficient for a successful measurement, resulting in 20 to 35 measurements per sample. Failed measurements were mostly the result of pollen grains torpedoing themselves out of sight when hit with the laser and by positioning of the pollen grains to close to the edge, so that not enough pollen are found in the central part of the plate. This would lead to no or a very low peak, with deviating values and a high standard deviation.

Table 2

Mean $\delta^{13}C_{pollen}$ of *Pinus* with their standard deviation, standard error and number of counts per sample

Age	$\delta^{13}C_{pollen}$	stdev	SE	counts
301.95	-27.35	1.23	0.27	21
310.587	-27.69	1.66	0.32	27
319.354	-26.48	1.33	0.22	35
333.045	-26.58	0.95	0.17	33
333.953	-27.44	0.90	0.16	32
346.832	-26.71	1.79	0.40	20
360.678	-27.39	1.12	0.21	29

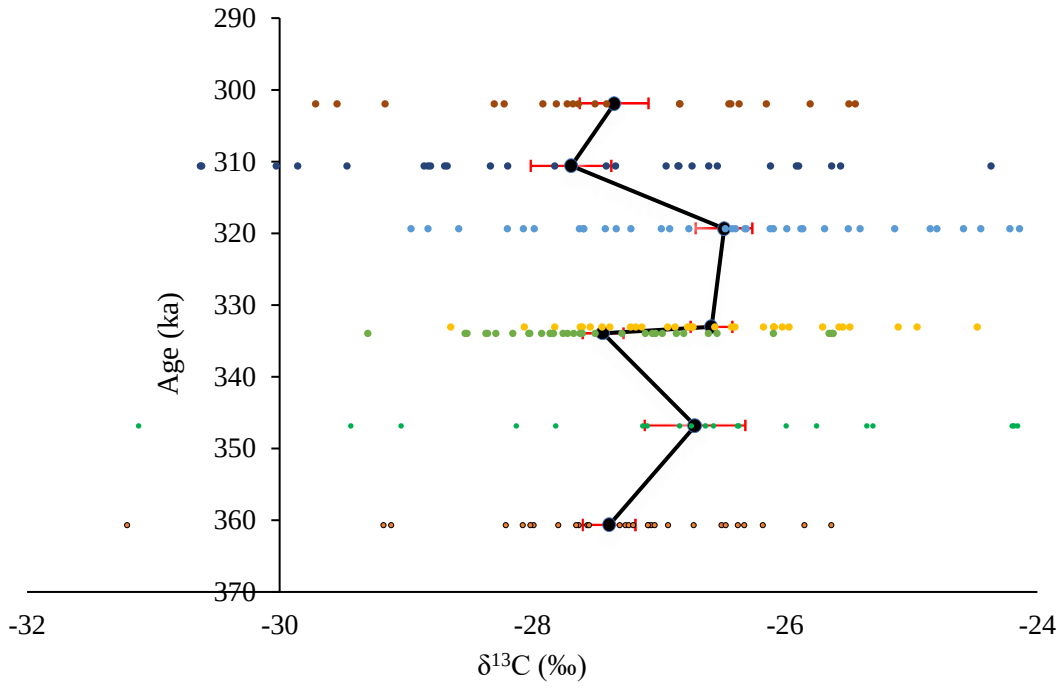

Figure 4: Averaged $\delta^{13}C_{pollen}$ values plotted against age. Red error bars show the standard error (Table 2), which is calculated as the standard deviation divided by the root of the total counts. The dots show the scatter of single measurements per sample.

The values of *Q. robur* and *Abies* pollen can also be found in Appendix 5. However, these had mixed results. Oak pollen were generally more depleted in $\delta^{13}C$ than *Pinus* pollen (mean of -28.17‰), but since *Q. robur* grains range from 20-30 µm, single grains yielded very small peak areas that greatly enhanced the standard deviation and troubled the viability of the measurements. The standard error (SE) was also 0.60 for *Quercus*, which is much higher than for *Pinus* (Table 2) and *Abies*, which was 0.20. The small occurrences of ablating multiple grains at once also resulted in low peak areas. The first sample only yielded 9 measurements, all with a low area and large standard deviation. The second sample was not analysed due to these practical problems.

These implications were enhanced by the susceptibility of *Quercus* pollen to fly away when hit with the laser, so that only a small part of the pollen grain is ablated. This occasionally happens with *Pinus* grains, only for *Quercus* grains its more the norm. This can possibly be avoided by pressing the nickel plates together with increased pressure. Furthermore, *Quercus* pollen are difficult to see under a binocular, so repositioning them to be in the central part of the nickel plate is tedious work and subsequently parts of the sample will be outside of the lasers effective reach. This part is quite vital for smaller pollen grains, as ideally, the pollen have to be positioned close together to allow multi-grain analysis. If the laser has to be activated for a long time to ablate multiple pollen grains at once, the chance of contamination by ablating the nickel base will increase.

Abies on the other hand, showed higher peak areas and less failed measurements. The mean $\delta^{13}C$ of the two samples was -24.70‰ and -26.91‰ respectively, so their $\delta^{13}C$ range is larger than that of *Pinus* grains, although the inter-pollen variability is similar (Appendix 5). *Abies* also produces pollen grains large enough to do multiple measurements on one grain. This offers the possibility to investigate intra-pollen variability. For every sample, six pollen grains were ablated twice to see intra-pollen variability, resulting in a difference of 0.02– 1.5‰. Most measurements showed a difference of less than 1‰ (Appendix 5). This also agrees with the results of van Roij et al., (2017) who measured intra-pollen variability on *Zea mays* and showed that single pollen are more homogeneous than different pollen grains. Both *Quercus robur* and *Abies* are however not consistently present in all samples and are therefore not suitable for reconstructing $\delta^{13}C$ over a continuous record.

5. Discussion

Comparison with terrestrial and marine proxies

The relative abundance of AP-*Pinus* pollen provides a good proxy for climate reconstructions and can be used in combination with biochemical proxies, like Total Inorganic Carbon (TIC, Fig. 5) and precipitation induced from speleothem and calcite $\delta^{18}O$. High TIC values characterize interglacials and indicate high photosynthetic induced rain of calcite by rising spring and summer temperatures and increased weathering by higher precipitation and meltwater rates. During glacials, when TIC values are low, siderite can form (Lacey et al., 2016), although these intervals were too low in resolution to use as a proxy for glacial variability. Weathering rates can also be stimulated during glacial periods, by less dense vegetation covers. Overall, more clastic material enters the lake basin during glacial periods. MIS 9 and 7 have lower TIC values, but higher Total Organic Carbon than MIS 11, implying colder conditions, with less evaporation (Francke et al., 2016). Oxygen isotopes measured from speleothem OH2, originating from a cave near Lake Ohrid, have a dominant precipitation signal (Regattieri et al., 2018), in which higher/lower values suggest drier/wetter conditions. Wetter

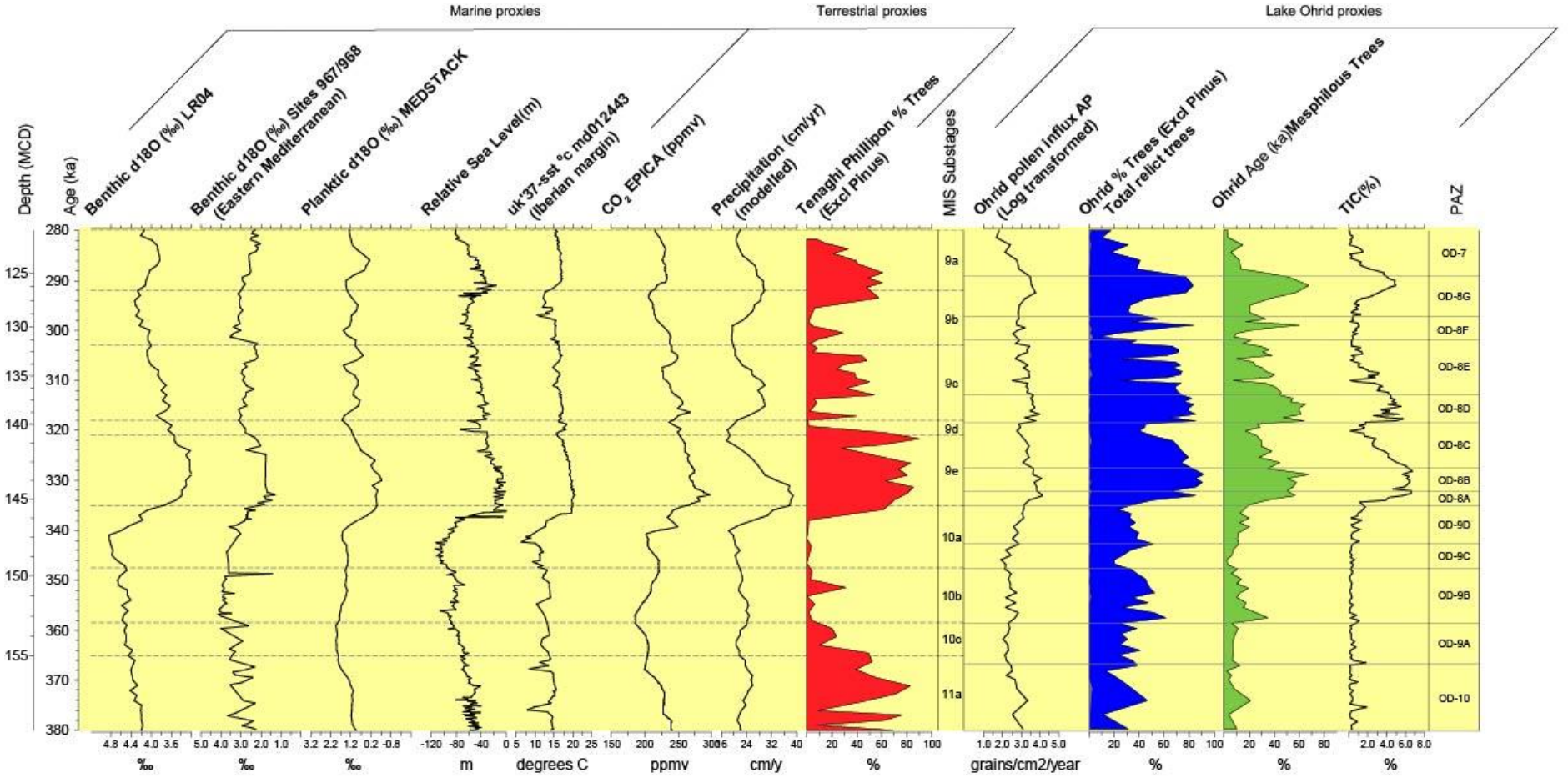

Figure 5: Comparison of several marine and terrestrial proxies against selected proxy data from Lake Ohrid. Marine and terrestrial data have been plotted against MIS substages that are discussed in the text, while Lake Ohrid proxies are plotted against pollen assemblage zones. Marine proxies: LR04 $\delta^{18}O$ benthic stack (Lisiecki and Raymo, 2005); stacked benthic $\delta^{18}O$ data for the eastern Mediterranean ODP sites 967 and 968 (Eastern Mediterranean, Konijnendijk et al., (2015); planktic $\delta^{18}O$ MEDSTACK data (Wang et al., 2010), reconstructed global sea-level (Rohling et al., 2009); $U^{k'}_{37}$ based sea surface temperatures from the Iberian margin from site MD01-2443 (Martrat et al., 2007). Atmospheric CO_2 reconstructions (Bereiter et al., 2015). Tenaghi Philippon: AP-*Pinus* % (Pross et al., 2015). Lake Ohrid proxies: AP-*Pinus* pollen influx (grains/cm^2/year); AP-*Pinus* percentages and mesophilous tree percentages (this study); simulated precipitation rates (Wagner et al., accepted); total inorganic carbon, TIC (Francke et al., 2016).

climates are also evident from $\delta^{18}O$ values of calcite at Lake Ohrid, which were the lowest during MIS 9 (Lacey et al., 2016).

The pollen record does show some controversy with respect to the exact transitions of the substages (Fig. 5, Appendix 6). This is also evident from the minor discrepancy between the pollen superzones constrained by Sadori et al., (2016) and the Marine Isotope Stages. The pollen record of Tenaghi Philippon (Pross et al., 2015) is dated relatively to the benthic isotope stack, hence their perfect match. The discrepancy in the Lake Ohrid pollen record can also indicate a lag in terrestrial response compared to the marine or ice core records, so readdressing this can shed new light on the issue.

Overall, the pollen zones broadly complement the pollen superzones defined by Sadori et al., (2016), except for OD-8A (Table 1). Sadori et al., (2016) place the transition of superzone OD-9 to superzone OD-8 at 333.5 ka, while the CONISS data in this paper defines the boundaries of OD-8A between 332.1 and 334.9 ka. This is in better agreement with the transition of MIS 10 to MIS 9, which has been put at 337 ka (Railsback et al., 2015). The forest expansion at the beginning of an interglacial period often lags behind the marine record, as these expansions are influenced by the June insolation peak, which causes different phasing between the onset of terrestrial and marine stages after a Termination deglaciation (Tzedakis et al., 2004). As a side note, OD-8A is based on only three samples, which is rather meagre. Still, this pollen zone marks the transition into AP dominated vegetation and is more similar to OD-8B than to OD-9D (Fig. 2).

The other boundaries as defined by Sadori et al., (2016) are consistent with the high resolution pollen data. The transition of MIS 11 to MIS 10 is put at 367 ka, which is in agreement with both Railsback et al., (2015) and Sadori et al., (2016). This interval has already been analysed for high resolution at Lake Ohrid and is on the same line is the samples studied here (Kousis et al., 2018). This record showed colder conditions for Lake Ohrid during this interval than at neighbouring sites Ioannina and TP, due to its higher altitude.

MIS 10 has not been documented in substages as much as MIS 9 and with only three substages in this period, is well comparable with the pollen record. As OD-9B (358.5-346.5 ka) shows an increase in montane taxa during this interval, alongside with the steady abundance of steppe taxa, the mild conditions of interstadial MIS 10b do correspond well to this period. The reoccurrence of *Abies* and *Picea* are indicative of wetter climate conditions, since these taxa do not fare well with dry conditions (San-Miguel-Ayanz et al., 2016). This transition is also in agreement with the transitions used by Lundberg and McFarlane (2007), which defined the substages for MIS 10 for the first time. The glacial vegetation agrees with other cores, (e.g. Lake Van, Litt et al., 2014), although the concentration of *Pinus* during MIS 10 is quite high compared to other glacial stages (Sadori et al., 2016). This can be caused by the presence of widespread thickets, or long transport distances.

In MIS 9, the pollen record agrees less with the substage definitions. This is also seen in other papers, that use the substages a bit differently (Appendix 6). MIS 9e is documented to have peak interglacial conditions (Lacey et al., 2016; Regattieri et al., 2018), which is supported by the pollen record and by peaks in the green algal genus *Botryococcus*, which is an indicator for increased productivity in the lake (Appendix 4). Temperate forests, mainly consistent of deciduous oaks, are present in multiple sites short after the start of the interglacial, but records also show low *Pinus* concentrations during this interval (Reille et al., 2000; Roucoux et al., 2006). Around 321 ka, at the end of OD-8C, colder conditions start to prevail across Europe, as is seen in decreases in AP-Pinus at the Iberian margin (Roucoux et al., 2006), Lake Van in Turkey (Litt et al., 2014) and Tenaghi Philippon (Tzedakis et al., 2006) and at Lake Ohrid. This

is also seen from decreasing *Abies* and *Picea* populations and pollen concentration at Lake Ohrid. Since this drop in pollen influx lasts until 318.7 ka and then becomes dominant again, it seems evident to link this small interval from 321-318 ka to stadial MIS 9d. This is supported by Lacey et al., (2016), as there is an increase in calcite oxygen isotopes showing less precipitation and by a massive drop in TIC values (Francke et al., 2016). Other proxies in Fig. 5 also recognize this event, where most proxies recover around 316 ka. On the other hand, Railsback et al., (2015) and Regattieri et al., (2018) define MIS 9d from 321-313 ka, based LR04 oxygen isotopes that depict unstable hydrology and slightly reduced precipitation for this period. Fig. 5 also shows that the benthic LR04 $\delta^{18}O$ record shortly recovers and then shows slightly increasing values from 312 until 305 ka.

What is interesting here, is that the simulated precipitation for Lake Ohrid (Wagner et al., accepted) and the AP-*Pinus* and mesophilous trees curve show a drop between roughly 321 and 318 ka, while *Pinus* concentrations express a slight lag and show lower values between 317 and 313 ka, which is indicative for drier periods (Fig. 5). Montane tree influxes are low from 321 to 313 ka. Furthermore, the pollen record from Tenaghi Philippon shows low AP-*Pinus* concentrations in the same interval (Pross et al., 2015).

After 318 ka, the AP-*Pinus* record shows high concentrations, with two short-lived contractions, until 303 ka, which relates to MIS 9c. A peak in benthic oxygen isotope values at 302.6 ka is most prominent from site 967/968, where the benthic LR04 record shows a more gradual increase starting from 300 ka (Fig. 5). Lacey et al., (2016) document a slow transition towards low $\delta^{18}O$ and low $\delta^{13}C$ values for calcite between 318 and 310 ka, which they relate to MIS 9c, while Regattieri et al., (2018) document wetter conditions between 313 and 306 ka, which is supported by their correlation of speleothem $\delta^{18}O$ and the pollen record of the Iberian margin (Tzedakis et al., 2004), although the end of MIS 9c in the pollen record is put at 299 ka for this site (Roucoux et al., 2006). Based on their pollen zones, that describe deciduous *Quercus*, *Pinus* and evergreen *Quercus* for this interval, Fletcher et al., (2013) define MIS 9c from 312-303 ka, but since their record starts at 312 ka, the start of MIS 9c could be earlier.

The early glacial of MIS 9b-a, starting from 303 ka, shows more variation in the AP-*Pinus* concentration and an initial reduction in precipitation. Since the high resolution interval ends at 297 ka, it is most likely that this period (303-297 ka) correlates to part of MIS 9b and that MIS 9a is younger and not present in this interval. This is in agreement with Railsback et al. (2015) and Lacey et al. (2016), that define the end of MIS 9b at ~292 ka (Appendix 6). This is based on lower precipitation rates, a break in TIC preservation and the formation of siderite (Lacey et al., 2016), and low concentrations in the TP pollen record, from 304-295 ka (Pross et al., 2015). A drop in $u^{k'}_{37}$ derived sea surface temperatures from the Iberian margin between 298 and 290.3 ka suggest the different placement of this stadial (Martrat et al., 2007). The small overlap of the high resolution record of Tenaghi Philippon can be of value for this interval (Fletcher et al., 2013) (Fig. 6). Close inspection of the two records shows that very similar peaks are present, offering important information on short-scale climate events, since they are persistent in both records. However, implications arise since the two records show a slight offset between each other. TP shows a drop in AP from 300-292 ka, while the drop in AP at Lake Ohrid lasts from 303-295 ka and agrees more with the SST data. Similar small offsets are visible for temperate and NAP taxa.

The TP pollen record is placed on the EDC3 Antarctic ice core timescale (Parrenin et al., 2007), based on comparison of Iberian margin SST (Martrat et al., 2007) and MD01-2443 pollen record, which is aligned with benthic $\delta^{18}O$ (Roucoux et al., 2006). Since this is not an independent age constraint for this site, small offsets with other sites are possible. This small

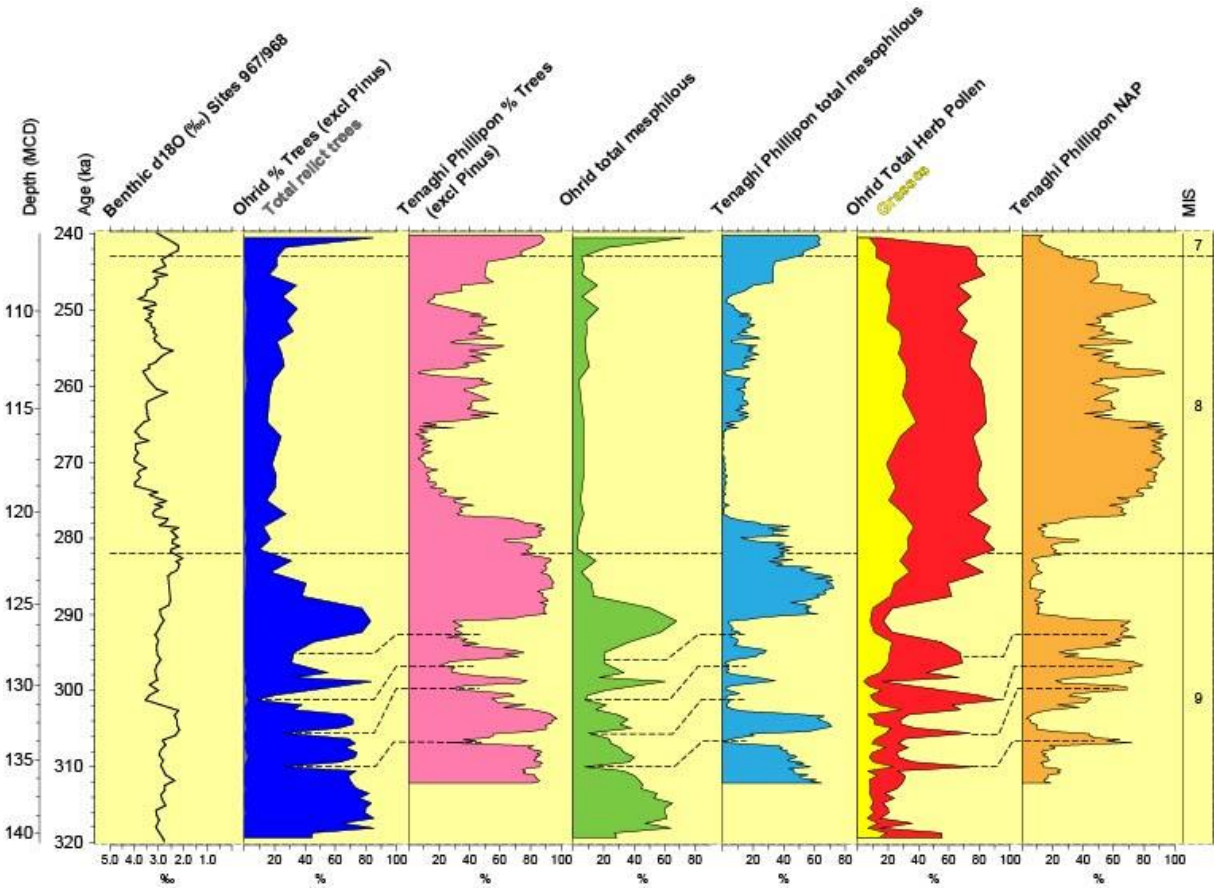

Figure 6: Correlation of Lake Ohrid and Tenaghi Philippon (Greece) data from Fletcher et al., (2013), for MIS 9 and 8. Dashed lines indicate interpreted correlation between the sites. Lake Ohrid data for MIS 8 is derived from Sadori et al., (2016).

offset between the two sites falls within the uncertainty of the age model and since peaks in the records correlate quite well, it is likely that these peaks show the same events (Fig. 6), which is also supported by the correlation between the TP record and speleothem data from Lake Ohrid (Regattieri et al., 2018). In their study, Fletcher et al., (2013) address more forest expansion events than the four main peaks found in their record. These smaller expansions correlate better with the Lake Ohrid record in terms of their dating, but are of much lesser extent and so likely indicate different events. Shifting the record from Lake Ohrid to match the TP record can create other problems with the correlations of other events. More insight on the Lake Ohrid age model can be achieved by pinpointing and matching high resolution forest expansion/contraction events of the Lake Ohrid pollen record to other proxies.

Millennial scale variation and link to North Atlantic

Determining rapid climate changes in this record is partially complicated due to the analysing methods, where the samples counted here are positioned in between the already studied samples. Possible differences in the counting method or sample preparation can result in differences between samples, since no subsequent samples have been counted by the same person. Since the same protocol is honoured during preparing and counting and similar pollen counts were realized, this implication is not very significant and rapid changes in the vegetation are not regarded as analytical errors.

Several rapid, short-term events can be identified in the AP-*Pinus* record (Fig. 5). During the glacial interval, one major forest expansion event is recognized at 357.5 ka (OD-9B), with a

high abundance of deciduous oaks. Forest expansions are caused by abrupt increases in warmth and moisture availability. This event, however, is only seen in one sample, where only *Q. robur* shows a rapid increase and could be classified as a counting artefact. Another rapid forest expansion event is found at 298.9 ka (OD-8F), where the AP-*Pinus* percentage rises from 20 to 83%. A similar event is seen at TP, called event B3 (Fletcher et al., 2013), along with event B2. These events are not seen in the marine isotope record nor the CO_2 concentration, but Regattieri et al., (2018) reports a drop in speleothem $\delta^{18}O$ at 297 ka, indicating wetter periods.

Fletcher et al., (2013) linked forest expansions in their pollen record from Tenaghi Philippon to Antarctic temperature maxima. This coincided with low dust fluxes and high atmospheric methane concentrations (Loulergue et al., 2008; Lambert et al., 2012), which are coupled to Dansgaard-Oescher events (Barker et al., 2011). This suggests interhemispheric coupling of millennial scale climate variability to ocean circulation by the see-saw effect. It also shows that Atlantic climate variability transmitted rapidly into the Mediterranean region. Fletcher et al., (2013) also argues that millennial scale climate events are most evident in periods with intermediate global sea level (between -80 and -60 m compared to present day sea levels) and thus intermediate ice volume, as seen in MIS 9. During MIS 10, the forest expansion event at 357.5 ka occurred with a sea level of <-90 m (Rohling et al., 2009; Fig. 5), so this does not hold up here, which suggests that this peak is indeed a counting artefact.

Short-term forest contractions are also present in the Lake Ohrid record and display drops in temperature and moisture availability. Sinopoli et al. (2018) linked forest contractions at Lake Ohrid during MIS 5 to Greenland ice sheet instability, as is evident from ice rafted debris (IRD) events. Ice sheet instability occurs when ice volume passes a certain threshold and is paired with perturbations in the Atlantic Meridional Ocean Circulation (AMOC). This threshold is by some believed to be a value of 3.5‰ on the benthic $\delta^{18}O$ stack (McManus et al., 1999). This has implications for the continental hydrology of the Mediterranean, resulting in drops in arboreal taxa. Kousis et al. (2018) reported forest contractions at Lake Ohrid during MIS 11, before IRD events were documented in the North Atlantic, showing that the terrestrial record responded to millennial climate changes before the marine record did.

Furthermore, Kousis et al. (2018) linked forest contractions with a North Atlantic marine counterpart to a slowdown of the AMOC. One major forest contraction event in their MIS 11 record was linked to orbital forcing as it coincided with a summer insolation minimum. In our interval, montane taxa seem to contain a precession signal, but other orbital forcing signals are not significantly present, which is also limited by the short length of the interval. For forest contractions that are not recognized in the marine record, chances are that short-term changes in atmospheric circulation have reduced moisture availability in the Mediterranean region and are therefore not documented in the marine proxy record. This is also seen at the Iberian margin, where millennial timescale forest contractions did occur during MIS 9d, which was also warmer and wetter than in the Balkan Peninsula (Roucoux et al., 2006). The SST at the Iberian margin does not show the same extent in rainfall reduction however, suggesting a possible decoupling between the North Atlantic conditions and continental hydrology during periods of low ice volume and relatively strong AMOC.

At Lake Ohrid, two main short-lived forest contractions are seen during MIS 9c (Fig. 5), at 310 and 305.7 ka. These short events are also evident in the TIC record (Fig. 5). Based on the correlation with the TP record (Fig. 6), the same forest contractions occur at Tenaghi Philippon around 306 and 301 ka (Fletcher et al., 2013), but their duration is longer (around 2 kyr). Regattieri et al. (2018) reports an abrupt reduction of precipitation at 310 ka, lasting 1 kyr, along with a reduction in rainfall that starts at 306 ka, but lasts until 298 ka. CO_2 concentrations and

the planktic $\delta^{18}O$ stack are low between 310 and 308 ka and indicate a short period of colder and drier conditions (Fig. 5)(Bereiter et al., 2015; Wang et al., 2010). The event at 310 ka can be linked to an IRD depositional event in the subpolar North Atlantic (McManus et al., 1999). This event can act as a control point for the age model, as it is evident from multiple proxies, although these proxies are mainly derived from the same site. Due to this match, the age model seems correct and the shifting the age model to match the offsets with the TP record brings life to more problems than it solves.

Long-term climate evolution

While these wet conditions prevailed during MIS 7, 9 and 11, younger intervals experienced drier conditions. In fact, calcite derived $\delta^{18}O$ from Lake Ohrid show their lowest values of the last 600 ka during MIS 9, indicative of high precipitation (Lacey et al., 2016), and the interstadial MIS 9e records the highest simulated precipitation values (Wagner et al., accepted). Other striking features of MIS 9, compared to other interglacial intervals, is the high SST at the Iberian margin (Martrat et al., 2007) (Fig. 5) and high atmospheric methane concentrations (Loulergue et al., 2008).

With regard to long-term climate variation, MIS 9 and 7 had different atmospheric regimes than following MIS, as the Mediterranean climate regime still influenced the area. With time, continental climate became more dominant and brought drier conditions (Buggle et al., 2013). This is evident from decreasing soil formation, by increased weathering from aridification.

Obreth et al. (2016) studied loess plateaus in the Southern Danube basin and investigated the relative influence of Mediterranean climate against continental climate as expressed by grain size and geochemical proxies, in which glacial periods were characterized by coarser grain sizes. MIS 9 and 7 show the presence of Cambisols, which have high clay content and are reddish of colour, showing a strong influence of Mediterranean climate, which weakened over time (Buggle et al., 2013). At Lake Ohrid, Mediterranean climate conditions are modified due to its altitude and distance from the sea, making it more sensitive to continental influences.

MIS 5 was the first interglacial with continental climate characteristics, probably related by Greenland ice sheet retreat during this period, causing more influence of the Siberian High at the Balkans (Obreht et al., 2016). This is not necessarily the case for Lake Ohrid, as the precipitation during MIS 5 is similar to MIS 9 (Wagner et al., accepted). Another explanation for this change in climate regimes argues that due to glacial isostatic rebound by glacial erosion of mountain ranges like the Alps and the Dinarides, westerlies are blocked, which reduces the precipitation and pushes the climate towards continental conditions (Buggle et al., 2013).

Link between pollen influx and atmospheric CO_2

To see what effect the global atmospheric CO_2, retrieved from Antarctic ice cores (Bereiter et al., 2015), is on the total concentration of pollen, the pollen influx of AP-*Pinus* is plotted against the CO_2 concentration (Fig. 7, Appendix 7). In the intervals where AP taxa dominated, the pollen concentration was generally high, while the concentration dropped in NAP dominated intervals.

Two outlier samples has been take out of this equation as it only had 3 AP counts (*Pinus* excluded). This resulted in a AP-*Pinus* concentration of 186 grains/g, while the rest of the samples show a concentration ranging from 1,720 to 387,215 grains/g. The pollen influx is calculated for AP-*Pinus*, *Pinus*, NAP and upland pollen (AP+NAP – *Pinus*). Due to the large fluctuations in pollen concentration, the pollen influx is log transformed. This compared to the EPICA CO_2 record shows a good match, especially for AP-*Pinus* and upland pollen, implying

that higher CO_2 concentrations result in an increase in pollen production. The other scatterplots display a correlation less optimal than the AP-*Pinus* curve, but still show the same trend (Appendix 7). This relation can possibly be used to infer paleo-CO_2 concentrations based on pollen influx.

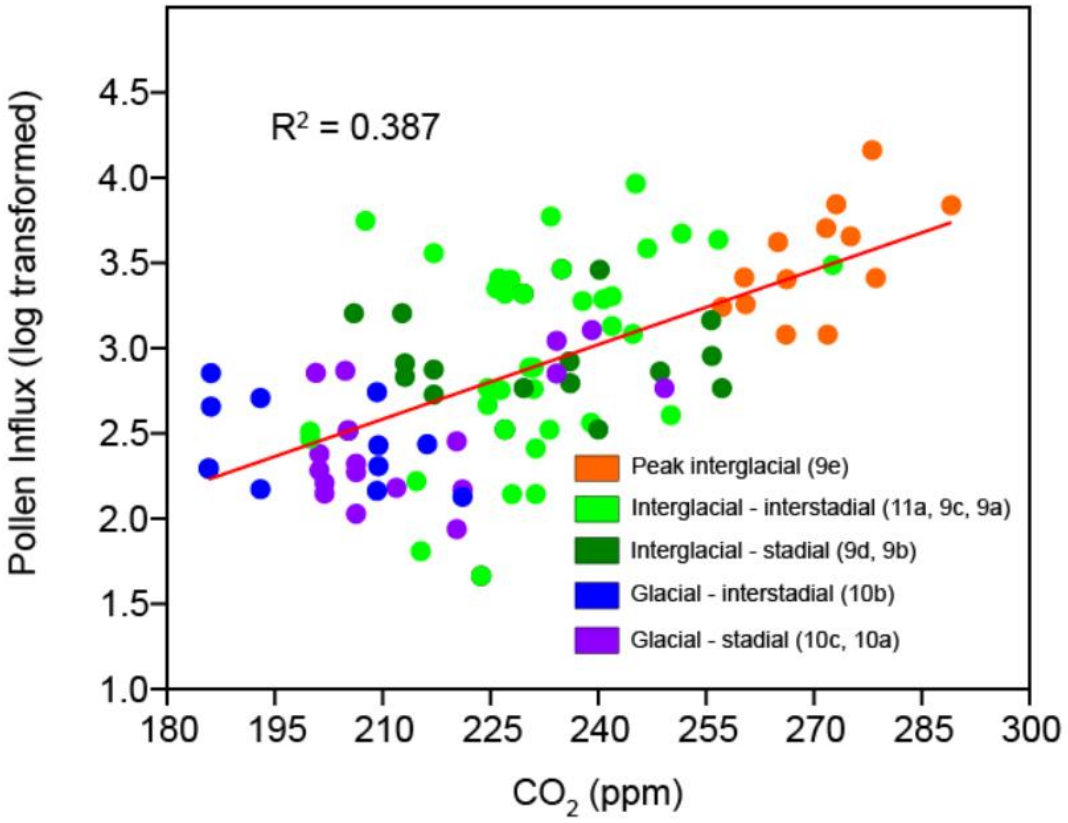

Figure 7: Scatterplot of log transformed AP-*Pinus* pollen influx against atmospheric CO2 concentrations (Bereiter et al., 2015), for all samples between 280 and 380 ka. The samples have been resampled to match the CO_2 record and MIS substages have been divided into five categories. Graphs made with Past (Hammer et al., 2001).

In Fig. 7, the data points are linked to MIS substages and are divided into five categories, to see if this link is visible during all climatic intervals. This shows, that certain intervals do not document this trend. For example, during MIS 10b, the pollen influx decreases with rising CO_2, while during the stadials of MIS 9, there is no significant rise in pollen production with different CO_2 levels. This complicates the correlation, as there seems to be no preference for certain intervals for this phenomenon, although the correlation seems to increase with higher CO_2 levels. Overall, the trend of a higher pollen influx with elevated CO_2 levels still holds and is also supported by other studies (e.g. Ziska and Caulfield, 2000), but on short intervals of generally 10 kyrs, this link seems more complex and should be studied before acclaiming this as a paleo-CO_2 proxy. On timescales of 100 kyr, which has been applied here, the correlation seems sufficiently evident that it supports the potential of pollen accumulation rates as a paleo-CO_2 proxy and that the standing biomass around the lake is thus CO_2 controlled. Uncertainties in the age model of the EPICA data can also result in a less optimal correlation, so this can possibly be improved for a better correlation. To increase our understanding of this relation, more data points are needed. In Fig. 7, not all categories consist of the same amount of samples, which can result in wrong interpretations. For example, MIS 11a, 9c and 9a are labelled as

warm periods during interglacials, but not the peak interglacial conditions that occur directly after a transition to an interglacial interval. This category has the most data points and subsequently also the largest scatter, so the addition of more data points can result in a different trend. With the data presented here, the correlation suggests a relation between increasing pollen influx and rising atmospheric CO_2, but this trend is less apparent with a small amount of datapoints.

Accuracy of carbon isotope measurements

Interpreting the $\delta^{13}C$ values of single measurements needs to be done with a certain amount of caution. As not all ablations succeed, some failed ablations can still result into small peaks and give values that perturbates the $\delta^{13}C$ signal from pollen. Peaks where little material is ablated often result in outlier values that shift the average $\delta^{13}C$ signal and generally increases the standard deviation. To avoid data manipulation, an objectively chosen threshold is needed to validate the measurements. This threshold is based on the difference between the height of the peak of a measurement and the background level. If a peak is 5 times as high as the background level, it shows a stronger signal and is more trustworthy than when the peak is only twice as high as the background. This is useful to objectively filter out failed measurements and . These failed measurements are often addressed during ablation and taken out of the data set, but this is complicated when grains only partially ablate or are located too close to the edge of the ablation chamber, as the edges are not well visible. Outlier data, which is most often more depleted in ^{13}C than the sample, can also be the result of ablation of the nickel base, which has an inconsistent peak of -30.74 ± 1.00‰ (van Roij et al., 2017). Applying a threshold filters the data and ensures that the remaining outlier data is a valid measurement, as some deviation in pollen $\delta^{13}C$ may reflect natural variability, which is estimated to be around 0.4-0.6‰ for inter pollen measurements (van Roij et al., 2017).

Furthermore, every PE measurement should at least have an area of >4 volt seconds (Vs), as at this point the standard deviation stabilizes at 0.41‰ (van Roij et al., 2017). This results in a more consistent signal after correcting with the PE. For most samples, these boundary conditions do not affect the measurements, but in two samples, the exclusion of five or six measurements results in a $\delta^{13}C$ shift of ~1‰ (Appendix 8). The impact of different thresholds on the carbon isotope data and how this influences the samples can be found in appendix 8.

The largest shifts are seen between 2 and 3 times the background signal. A higher threshold does generally decrease the standard deviation, so using a stricter threshold should raise the confidence level, at the expense of a mean $\delta^{13}C$ signal based on less individual measurements. The difference between a threshold of 3.5 or 6 times the background signal lowers the standard deviation a bit by excluding several measurement, but does not affect the mean $\delta^{13}C$ value in a major way (Appendix 8). Above 6, the amount of measurements per sample becomes critically low, which inhibits the confidence of the mean $\delta^{13}C$ value. If there is enough sample, for instance if multiple *Pinus* grains could be ablated at once, a higher cut-off point would increase the credibility of the measurement. For example, Nelson (2012) used a minimum of 1.2 Vs per measurement to ensure an accuracy and precision of < 1‰, while analysing *Artemisia* pollen. Implementing this threshold for single *Pinus* grains in this study, only 0-3 measurements per sample would be valid, which does not result in feasible results. Another downside to measuring multiple pollen grains at once is that this results in a mixed signal, where inter-pollen variation might be obscured.

The danger of establishing such a threshold lies at defining the boundary between natural variability and mechanical inconsistency. Placing the boundary too high might exclude some

natural variability between pollen grains and skews the results. During measurements, successful ablations could result in a peak between 3.5 and 6. Due to these successful ablations, there is no reason to exclude them here, as this would lower the measurement count and would take away data from a good measurement. So, to include these data and since the data remains relatively constant after using higher thresholds, the boundary condition is put at 3.5 (Appendix 5). This threshold is also applied to Fig. 4.

Using the threshold of 3.5 results in the exclusion of all *Q. robur* measurements, which combined with the other complications that occur when analysing *Q. robur* pollen grains makes them unsuited for this analysis in this setting. It can still be used, but the amount of pollen grains needed to make sufficient measurements on multiple grains likely exceeds the content of most pollen samples, or greatly increases the isolation process. *Q. robur* pollen were selected as pilot samples in the first place for their high abundances in certain samples and since *Pinus* pollen can be transport for long distances due to their wind-pollination and their bisaccate morphology, possibly diluting the local signal. On the other hand, a small proportion of all pollen grains are susceptible to travel large distances (Hjelmroos and Franzén, 1994), so this does not mean that *Q. robur* pollen are per se from the source area.

Abies pollen are large enough to ensure that plentiful mass is ablated and with the possibility of two measurements on one grain. These values showed that pollen grains are more homogeneous than different pollen grains. Van Roij et al., (2017) showed that the standard deviation of these measurements is lower than the standard deviation of the PE, so that at this scale, pollen grains are virtually homogeneous. Not all of the data collected here agree with that, as the standard deviation of the *Abies* samples are within the same range as the *Pinus* samples, except for one *Abies* sample which showed a standard deviation of 0.6 when only considering double measured pollen grains. This difference also shows that natural variation between pollen grains can occur and do not exist merely by analytical errors.

Interpretations $\delta^{13}C_{pollen}$

The changes in the $\delta^{13}C$ of pollen on its own is difficult to interpret when compared to atmospheric CO_2 levels. To get a grip on whether this signal represents ambient atmospheric CO_2 concentrations or the physiological response of plants to changing climate conditions, the $\delta^{13}C_{pollen}$ needs to be converted. A useful tool to investigate the response of C3 plants to fluctuating atmospheric CO_2 concentrations is the ratio between intercellular CO_2 and atmospheric CO_2 (c_i/c_a ratio). This ratio is dimensionless, as both c_i and c_a are expressed in ppm, and is driven by the demand of CO_2 for photosynthesis (A) and supply through stomatal conductance (g_{sc}). Under optimal conditions, the diffusion of CO_2 through stomata equals the biochemical intake of CO_2 through photosynthesis, which is assumed as steady state. The $\delta^{13}C$ fractionation increases with a decreasing c_i/c_a ratio, if the c_i/c_a ratio would be 1, no fractionation takes place. As c_a changes over glacial-interglacial timescales, the behaviour of c_i can give valuable information on the response mechanisms plants use with changing CO_2.

Intercellular CO_2 (c_i) can be influenced by factors such as temperature, moisture availability and nutrient access, as this regulates photosynthesis. Especially the amount of N in the leaves is important, as photosynthetic enzymes make up a large portion of nitrogen in leaves. Many studies suggest that c_i is mostly dependent on mean annual precipitation (MAP), as this controls the stomatal conductance and photosynthesis rates (Kohn, 2010; Hare et al., 2018). However, this relation seems nonlinear. $\delta^{13}C$ values of C3 plants average around -28.5‰, where -22‰ or more positive is characteristic for arid areas and -31.5‰ or more negative for tropical canopies (Kohn, 2010).

The physiological response of plants for c_i relative to c_a is not always similar and can be grouped into three strategies (Saurer et al., 2004): (a) maintaining a constant c_i relative to changing c_a, (b) maintaining a constant drawdown of CO_2 (constant c_a-c_i) and (c) maintaining a constant c_i/c_a ratio. These strategies are based on their water use efficiency, which is the ratio between photosynthetic carbon assimilation and water loss via stomatal conductance. Maintaining a constant c_i/c_a ratio is predicted as the most optimal way to balance carbon assimilation and water transport (Prentice et al., 2014), while a constant c_i and c_a-c_i is biased towards a higher and lower than optimal water use efficiency, respectively. Simply put, a higher water use efficiency tends to use less water with increasing CO_2, to counter drought stress. Generally, a higher atmospheric CO_2 concentration results in increased photosynthesis and intrinsic water use efficiency, i.e. a higher A/g_{sc} ratio.

Many studies that use this ratio are focussed on recent timescales and the response of vegetation on the rapid CO_2 emissions of the present day (e.g. de Boer et al., submitted). Studies that do go back in the geological record are mostly restricted to the last glacial-interglacial cycle, while measurements of $\delta^{13}C$ of CO_2 go back only 150 kyr (Köhler et al., 2010). Studies that use older material are mainly focussed on the relation between intercellular CO_2 and tooth enamel, to reconstruct paleo-diets of certain animals (Hare et al., 2018).

To calculate the c_i/c_a ratio, beside the $\delta^{13}C$ of pollen, also the $\delta^{13}C$ of CO_2 is needed. Changes in $\delta^{13}C$ of atmospheric CO_2 on glacial-interglacial timescales are related to changes in terrestrial carbon storage and, in lesser amount, to ocean-related processes, such as biological pump efficiency and upwelling (Köhler et al., 2010). During glacial-interglacial transitions, the $\delta^{13}C_{CO2}$ can drop by -0.2‰, before slowly returning to previous values. As far as is known, long-term variability is nearly absent, as all factors influencing $\delta^{13}C_{CO2}$ cancel each other out on 100 kyr timescales. Unfortunately, no measured records are available for MIS 9 and 10, so for the sake of this study, we use values based on a long transient carbon cycle model for the $\delta^{13}C$ of atmospheric CO_2 by Köhler et al. (2010).

By using the measured $\delta^{13}C$ of the pollen grains and the modelled $\delta^{13}C$ of CO_2 from Köhler et al., (2010), the degree of carbon discrimination by plants, $\Delta^{13}C$, can be calculated (Farqurah et al., 1982; Brienen et al., 2011):

$$\Delta^{13}C\ (‰) = (\delta^{13}C_{CO2} - \delta^{13}C_{pollen})/(1 + (\delta^{13}C_{pollen}/1000)) \qquad (1).$$

Since there is a linear relation between these components, the carbon discrimination can then be used to calculate the c_i/c_a ratio by this equation:

$$\Delta^{13}C\ (‰) = a + (b - a)c_i/c_a, \qquad (2)$$

where a (4.4‰) and b (28‰) are constants representing the magnitude of fractionation during gaseous diffusion and fractionation of CO_2 in C3 plants by Rubisco, respectively.

c_i (ppm) can be calculated by multiplying c_i/c_a with c_a, in which c_a is the atmospheric CO_2 from EPICA ice cores (Bereiter et al., 2015). These equations have been performed on every measurement of a sample, rather than the average $\delta^{13}C_{pollen}$ of a sample. For visualisation, the c_i response relative to rising c_a with a constant c_i/c_a is expressed by Δc_i, which is calculated as the difference of the initial c_i and a default c_i calculated with a constant c_i/c_a ratio and should thus be zero with a constant c_i/c_a.

The calculated c_i/c_a ratio, the c_i and the Δc_i are displayed in Table 3. The c_i/c_a ratio ranges from 0.70 to 0.75 and is quite constant, showing that the internal CO_2 of a plant is regulated by

changing atmospheric CO_2 conditions and follows the same trend (Fig. 8). Δc_i is multiplied by ten.

Table 3

Calculated values for c_i/c_a, c_i (CO_2 in leaf) and Δc_i, against the age, the atmospheric CO_2 concentration (Bereiter et al., 2015), measured $\delta^{13}C_{pollen}$ values, modelled $\delta^{13}C_{CO2}$ values (Köhler et al., 2010) and simulated precipitation rates for Lake Ohrid (Wagner et al., accepted).

Age (ka)	c_a (CO_2 in atm, ppm)	$\delta^{13}C_{pollen}$ (‰)	$\delta^{13}C_{CO2}$ (‰)	c_i/c_a	c_i (CO_2 in leaf, ppm)	Δc_i	*Precipitation (cm/year)*
301.95	239.00	-27.35	-6.70	0.74	178.01	1.29	19.40
310.587	223.20	-27.69	-6.69	0.76	177.43	5.00	29.98
319.354	233.40	-26.48	-6.72	0.70	164.22	-8.36	19.68
333.045	272.60	-26.58	-6.57	0.71	194.86	-6.70	38.71
333.953	282.40	-27.44	-6.58	0.75	213.07	4.26	38.15
346.832	204.80	-26.71	-6.64	0.72	147.03	-4.40	21.53
360.678	186.10	-27.39	-6.72	0.75	138.79	1.19	21.84

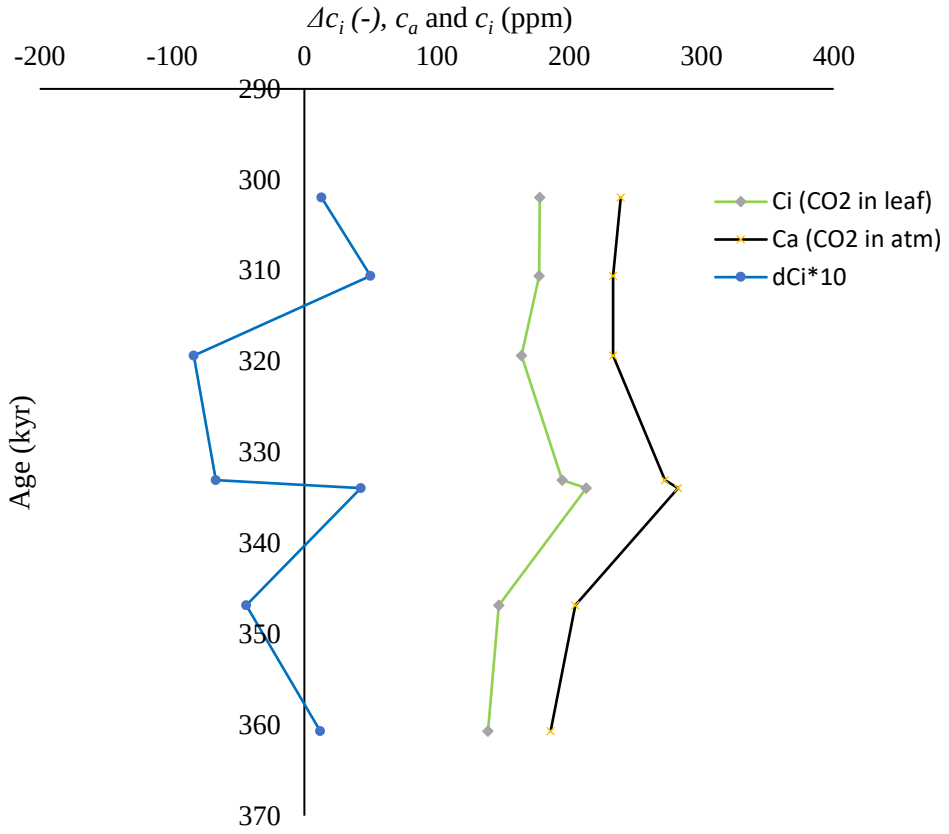

Figure 8: c_i, c_a and Δc_i plotted against age (ka). Δc_i is multiplied by 10 for visualisation.

The constant c_i/c_a ratio implies that *Pinus* adapts their stomatal conductance and photosynthetic capacity, to keep up with changing c_a. Assuming a correct $\delta^{13}C$ of atmospheric CO_2, *Pinus* had a standard CO_2-resonse, likely reflecting an increase in photosynthesis and less evaporation on the leaf level, so a slightly lower stomatal conductance.

The small changes that occur in Δc_i can occur due to varying conditions in moisture availability. A rise in Δc_i can be interpreted by higher stomatal conductance and photosynthesis

(transpiration) and/or lower photosynthetic capacity with regards to a constant c_i/c_a response, which is the default response to rising CO_2, with higher photosynthesis and slight closure of the stomata. Photosynthetic capacity is the maximum rate leaves can incorporate carbon during photosynthesis, under optimal conditions. It is expressed by the biochemical capacity (A_{bc}), which is the biochemical uptake of CO_2 during photosynthesis. It is limited by the carboxylation capacity and electron transport capacity and is also sensitive to nitrogen availability (Hopkins and Hüner, 2009), as this influences the carboxylation capacity. Under low CO_2 concentrations, the carboxylation capacity limits the maximum photosynthesis rate, while the acceptor molecule, RuBP (Ribulose 1,5-Biphosphate), is saturated, indicating inefficient use of resources. On the contrary, under high CO_2 concentrations or low light, the generation of the acceptor molecule would limit the photosynthetic capacity and the excess of carboxylation would express inefficiency. The variation in these two parameters provides important genotypic and phenotypic information (Farquhar et al., 1980). For a steady state assumption, the biochemical uptake of CO_2 must equal the diffusion of CO_2 through leaves, i.e. the stomatal conductance (Fick's law of diffusion). Both these processes are influenced by the internal CO_2 concentration in the leaves (c_i, Fig. 9) A rise in biochemical capacity lowers the c_i, but increases the photosynthesis. On the other hand, the c_i can also be lowered by lower stomatal conductance and a lowering of photosynthesis. With only $\delta^{13}C$ data, it is not possible to unravel which one of these two adaptations occurs.

A lower Δc_i reflects lower stomatal conductance and photosynthesis or higher photosynthetic capacity. This implies more drought stress and therefore a higher water use efficiency. Increased drought stress can be the result of warming induced increase in vapour pressure deficit, which is the atmospheric demand for moisture compared to its saturation level.

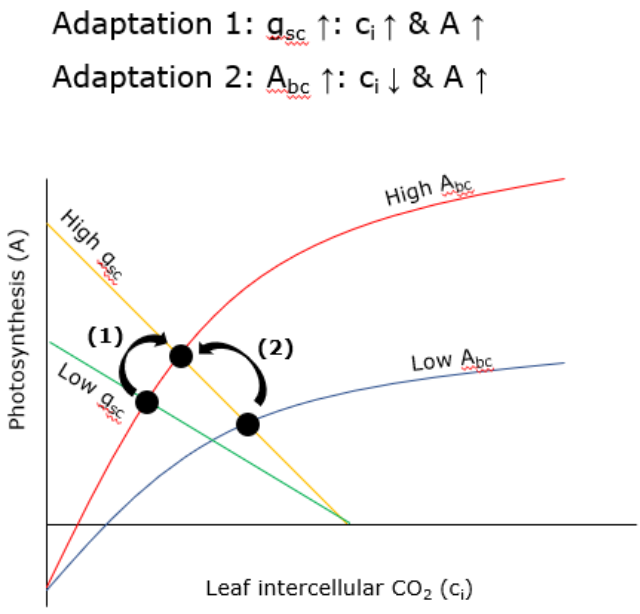

Figure 9: Possible responses of plants to variations in intercellular CO_2 or photosynthesis. For this model, it is assumed that the diffusion of CO_2 through the leaves – which equals the stomatal conductance (g_{sc}) due to Fick's law of diffusion – equals the biochemical uptake of CO_2. This biochemical uptake (A_{bc}) is controlled by the maximum rate of carboxylation and electron transport. Due to this steady state, in which g_{sc} equals A_{bc}, a rise in g_{sc} would increase the intercellular CO_2 and also increase the photosynthesis, as adaption 1 shows. If the biochemical uptake increases, c_i decreases, but photosynthesis increases again. Derived from de Boer (personal communication), as simplified version from the model of Farqurah et al., (1980).

The rise in Δc_i between 345 and 333 ka and between 320 and 310 ka suggests higher photosynthetic rates and stomatal conductance, corresponding with wetter periods. The lower Δc_i values between 333 and 320 ka could indicate drought stress, although the simulated precipitation values for Lake Ohrid do not show a decrease in precipitation around this time (Table 3). Furthermore, rainfall as induced from speleothem isotopic data (Regattieri et al., 2018), shows that 325-321 ka had the highest rainfall amounts associated with MIS 9e. This would imply that photosynthetic rates were high, as the stomatal conductance is not limited by drought stress. Another cause can be inaccuracies in the CO_2 record. A drop in precipitation is seen for the period of 321-318 ka (Wagner et al., accepted), which also shows low Δc_i values, so for this period drought stress could decrease the stomatal conductance and photosynthetic rates. Conifers are relatively sensitive to drier conditions, since they try to minimize embolism in the stem, which results in wide hydraulic safety margins. This causes conifers to close their stomata earlier when exposed to drought and thus reduced photosynthesis (Meinzer et al., 2009; de Boer et al., submitted). Drought reduces the stomatal conductance and transpiration and thus tree growth. Putting this much weight on a few measurement points is, however, not desirable. Ideally, a higher resolution record could grant a better interpretation for comparing the Δc_i to precipitation values, as now the interpretation is based on a few high or low measurements.

Within the light of present day carbon emissions, the effect of a higher pCO_2 on $\delta^{13}C_{pollen}$ has been an interesting topic of research (e.g. Kohn et al., 2010; Hare et al., 2018). For example, Brienen et al., (2010) showed that the tropical tree *Mimosa acantholoba* kept its c_i constant with rising CO_2, resulting in a drastic increase of water use efficiency of 40%, due to reductions in stomatal conductance. This also implies that photosynthetic rates did not increase with higher CO_2 concentrations. This strategy seems more often applied in semi-arid conditions, since it mostly conserves soil moisture. Moreover, measured rates of -1.7‰ /100 ppmv on 720 samples of wood cellulose from the Northern Hemisphere during the last deglaciation has been recorded for gymnosperms, so more negative values coincide with rising CO_2 (Hare et al., 2018). On the other hand, fossil collagen only showed a decrease of 0.3‰/100 ppm (Kohn, 2010). Within a glacial-interglacial cycle, the range of pCO_2 can get up to 100 ppm, especially with the high atmospheric CO_2 values of MIS 9. The change of -1.7‰ is not visible in our data, where an atmospheric CO_2 difference of nearly 100 ppm only shows a $\delta^{13}C_{pollen}$ difference of -0.05‰ (Table 3).

Furthermore, with the resolution used here, there is no confident trend visible in the comparison of $\delta^{13}C_{pollen}$ and atmospheric CO_2, but it seems that c_i follows the atmospheric CO_2 curve quite well. This suggests that the combination of $\delta^{13}C_{pollen}$ and $\delta^{13}C_{CO2}$ is dependent on the c_a, but that for $\delta^{13}C_{pollen}$, also other biochemical processes could be in play. There also seems to be a resemblance between Δc_i and the modelled precipitation rates (Table 3).

Modelled studies showed higher divergence during periods with low pCO_2 and argue that atmospheric effects on photosynthetic fractionation are then amplified (Hare et al., 2018). They also concluded that the during the last glacial cycle, changes in the terrestrial $\delta^{13}C$ mainly reflects changes in pCO_2, with small contributions of MAP.

It is difficult to confidently put a conclusion to this data, as the trend that is shown by Δc_i is hard to interpret with changing atmospheric CO_2. Furthermore, the uncertainties that arise by using modelled $\delta^{13}C_{CO2}$ can also obscure a possible strong response on changing atmospheric CO_2 concentrations, although this effect is quite small, as the $\delta^{13}C_{CO2}$ only varies between 0.2-0.4‰ on long time scales (Köhler et al., 2010). Interpreting and comparing the c_i/c_a ratio with fluctuating CO_2 levels is very difficult, since it is not possible with this information to separate the CO_2 signal and the hydrology signal, so the relative influence of the different factors that

alter the c_i/c_a remains largely illusive. Nevertheless, comparison of the c_i/c_a with other climate proxies such as precipitation can explain changes in this ratio. As it remained fairly constant in our results, interpretations can be made on the similarity of the trend between c_i and c_a and on photosynthesis and stomatal conductance rates, if CO_2 levels did not fluctuate. Other factors that could stimulate plants to adapt their internal biochemistry, for example nutrient availability, could also play a role and must be considered as well for a more complete picture.

Additional analysis of dual isotopes, by also measuring δ^{18}O-cellulose, can be helpful to investigate water sources, such as stomatal conductance, transpiration and the vapour pressure deficit (de Boer et al., submitted), but this his is unfortunately not feasible for pollen at this moment. An expansion towards coupled analysis with deuterium isotopes could possibly help unravel these responses to CO_2.

This new setup of measuring carbon isotopes on pollen grains sheds light to a different part of vegetation response on climatic forcing and adds valuable information in on long-timescale terrestrial climate reconstruction. Although uncertainties in the CO_2 concentrations and $\delta^{13}C_{CO2}$ can implicate the interpretation, the calculated c_i/c_a ratio shows a clear trend, in which c_i parallels c_a. The resulting constant c_i/c_a ratio is a logical response of C3 plants to atmospheric changes, so this confirms that the measured $\delta^{13}C_{pollen}$ represent trustworthy values that can be used to investigate adaptation techniques of C3 plants. Additionally, it may also act as proxy for atmospheric CO_2 concentrations, if the c_i/c_a ratio is known. Further research on higher resolution can study the link between Δc_i and precipitation with more detail and possibly reveal trends that are important for understanding these physiological mechanics that plants use under changing CO_2. Another adaptation of these carbon measurements can be the research on many different pollen taxa from the same age and the same atmospheric conditions, to unravel possible variations between plant taxa to the same forcing mechanisms, provided that sufficient pollen material is present for the selected taxa. These options offer a new window of research on vegetation dynamics on glacial-interglacial timescales, while the setup is also applicable to other small carbon containing particles.

6. Conclusion

The high resolution pollen record of Lake Ohrid provides new information on vegetation changes in the Balkan Peninsula during MIS 9 and 10 (297.5-370 ka). The increase in resolution makes it possible to identify and address millennial scale climate events during this period. The pollen record shows good correlation with biochemical proxies, the marine isotope stacks and nearby pollen records, implying a vegetation response to temperature and moisture availability. Based on the pollen record, MIS substages have been allocated to pollen zones, which overall correlate well with the marine record. MIS 10 was characterized by steppe concentration, with a small period of slight reforestation in between. The rise in AP that started at 335 ka marks the glacial-interglacial transition. MIS 9 showed high AP abundances through most of the interval, with a wide variety in AP taxa. The occurrences of now extinct taxa (e.g. *Carya*, *Pterocarya*, *Zelkova*) during this interval supports the earlier implied notion that Lake Ohrid acted as a glacial refugium for temperate trees.

Short-lived colder intervals during MIS 9 were present between 321-318 ka and at 310, 305.7 and 301 ka. These intervals were related to changing moisture availability due to instability of the Greenland ice-sheet and slowdown of the AMOC. Evidence of low precipitation rates during these intervals is available from speleothem oxygen isotopes and supports this. The forest expansion event at 298.9 ka can be linked to Antarctic temperature maxima and coincide with the occurrences of Dansgaard-Oescher events (Fletcher et al., 2013), showing

interhemispheric coupling. Some millennial time scale events are only recognized by local Lake Ohrid proxies such as precipitation and TIC and show that rapid changes in atmospheric circulation can drive variations in moisture availability in the Mediterranean, that are not seen in the marine record.

Comparisons of the pollen influx and the atmospheric CO_2 resulted in a good match, indicating that more pollen are produced under higher CO_2 concentrations, likely as a result of pollen productivity and population increases. With only a few data points, this trend is less clear and should be evaluated with more caution, but on longer timescales, this shows that the pollen influx can be a potential new atmospheric CO_2 proxy.

The experiment with measuring carbon isotopes on pollen grains of *Pinus* has shown exciting results. The abundance of *Pinus* grains in the record and its size allows analysis on single grains, as overall the signal fits well within the analytical confidence level. Analysis on smaller grains is possible, but tedious work due to the extra amount of grains needed and a complex repositioning process, as multiple grains have to be ablated within the same measurement. By converting these values into the c_i/c_a ratio, the physiological response of plants has been investigated. The resulting constant c_i/c_a trend implies a standard response to changing CO_2 concentrations, by increasing photosynthetic rates and lowering the stomatal conductance, so that less evaporation occurs on the leaf level, when CO_2 rises. Due to uncertainties in the CO_2 concentrations, $\delta^{13}C_{CO2}$ and interpretation of the c_i/c_a with changing atmospheric CO_2, these values remain difficult to interpret, but the clear trend of constant c_i/c_a shows that there is a logical response of the vegetation and that the measured carbon isotopes are trustworthy.

Acknowledgements

So, this is it then, you have reached the ending of this thesis. 30+ pages of pollen talk, so props of you are still reading this, which means you either really fancy pollen, or somehow feel pity for me. Hopefully you didn't catch hay fever on the way. Nevertheless, I hope it was worth the read and that you go on with your day, refreshed and inspired with new insights on life. Greatness is rarely accomplished alone, and also for this piece of work, I have had the pleasure of working with a great bunch of people, who all deserve to be praised for their respective roles in forming this thesis.

I want to thank the palynological team of Lake Ohrid, for retrieving the samples and giving me a lot of reference material. Without the samples, I would have had to use a lot more imagination than is probably allowed in the academic world. My gratitude also goes out to Giovanni and Natasja for their help during the lab process, Linda and Joost for their help with the preparation of my samples, operating the laser and the discussions on the reliability of my results. Also thanks to Hugo, for his interesting ideas on how to interpret these results.

Special thanks to Timme, for setting up this project and helping me along the way with pollen identification, steering this project in the right direction and providing me with constructive feedback. I hope that this thesis contributes to the Lake Ohrid project and that the carbon isotope technique helped with paving the way to new research opportunities. I am grateful to my fellow master students that also worked on their thesis this year, for providing me with motivation and a healthy mix of informal activities. Same goes out to the paleo-ecology group in Utrecht, which have kept me up to date on current affairs and the state of the cafés on the Uithof. Much obliged.

At last, I want to thank the reader, for taking the time to look at my work, as its nice to see that my thesis is used for more than improving my own learning curve. So, now that this is all done, time for a beer. Cheers.

References

Albrecht, C., & Wilke, T. (2008). Ancient Lake Ohrid: biodiversity and evolution. *Hydrobiologia*, *615*(1), 103.

Barker, S., Knorr, G., Edwards, R. L., Parrenin, F., Putnam, A. E., Skinner, L. C., ... & Ziegler, M. (2011). 800,000 years of abrupt climate variability. *science*, *334*(6054), 347-351.

Baumgarten, H., Wonik, T., Tanner, D. C., Francke, A., Wagner, B., Zanchetta, G., ... & Nomade, S. (2015). Age-depth model of the past 630 kyr for Lake Ohrid (FYROM/Albania) based on cyclostratigraphic analysis of downhole gamma ray data.

Bazin, L., Landais, A., Lemieux-Dudon, B., Toyé Mahamadou Kele, H., Veres, D., Parrenin, F., ... Loutre, M.F., 2013. An optimized multi-proxy, multi-site Antarctic ice and gas orbital chronology (AICC2012): 120–800 ka. Clim. Past 9 (4), 1715–1731.

Bereiter, B., Eggleston, S., Schmitt, J., Nehrbass-Ahles, C., Stocker, T. F., Fischer, H., ... & Chappellaz, J. (2015). Revision of the EPICA Dome C CO2 record from 800 to 600 kyr before present. *Geophysical Research Letters*, *42*(2), 542-549.

Bertini, A., Sadori, L., Combourieu-Nebout, N., Donders, T. H., Kouli, K., Koutsodendris, A., ... & Peyron, O. (2016). All together now: an international palynological team documents vegetation and climate changes during the last 500 kyr at lake Ohrid (SE Europe). *Alpine and Mediterranean Quaternary*, *29*(2), 201-210.

Beug, H. J. (1961). *Leitfaden der Pollenbestimmung für Mitteleuropa und angrenzende Gebiete: Lieferung 1*. Gustav Fischer Verlag.

de Boer, H. J., Robertson, I., Clisby, R., Loader, N. J., Gagen, M., Young, G. H. F., Wagner-Cremer, F., Hipkin, C. R., McCarroll, D. (submitted). Tree ring isotopes suggest atmospheric dying limits temperature-growth responses of treeline bristlecone pine.

Brienen, R. J., Wanek, W., & Hietz, P. (2011). Stable carbon isotopes in tree rings indicate improved water use efficiency and drought responses of a tropical dry forest tree species. *Trees*, *25*(1), 103-113.

Buggle, B., Hambach, U., Kehl, M., Marković, S. B., Zöller, L., & Glaser, B. (2013). The progressive evolution of a continental climate in southeast-central European lowlands during the Middle Pleistocene recorded in loess paleosol sequences. *Geology*, *41*(7), 771-774.

Burns, R. M., & Honkala, B. H. (1990). *Silvics of north America*(Vol. 2, p. 119). Washington, DC: United States Department of Agriculture.

Ceulemans, R., & Mousseau, M. (1994). Tansley Review No. 71 Effects of elevated atmospheric CO2on woody plants. *New phytologist*, *127*(3), 425-446.

Cheddadi, R., Guiot, J., & Jolly, D. (2001). The Mediterranean vegetation: what if the atmospheric CO2 increased?. *Landscape ecology*, *16*(7), 667-675.

Coplen, T. B., Brand, W. A., Gehre, M., Gröning, M., Meijer, H. A., Toman, B., & Verkouteren, R. M. (2006). New guidelines for δ 13C measurements. *Analytical Chemistry*, *78*(7), 2439-2441.

Cvetkoska, A., Jovanovska, E., Francke, A., Tofilovska, S., Vogel, H., Levkov, Z., ... & Wagner-Cremer, F. (2016). Ecosystem regimes and responses in a coupled ancient lake system from MIS 5b to present: the diatom record of lakes Ohrid and Prespa.

Descolas-Gros, C., & Schölzel, C. (2007). Stable isotope ratios of carbon and nitrogen in pollen grains in order to characterize plant functional groups and photosynthetic pathway types. *New Phytologist*, *176*(2), 390-401.

Donders et al., (in preparation).

Faegri, K., & Iversen, J. (1989). 1989: Textbook of pollen analysis . Chichester: John Wiley.

Farris, M. A., & Mitton, J. B. (1984). Population density, outcrossing rate, and heterozygote superiority in ponderosa pine. *Evolution*, *38*(5), 1151-1154.

Farquhar, G. D., von Caemmerer, S. V., & Berry, J. A. (1980). A biochemical model of photosynthetic CO 2 assimilation in leaves of C 3 species. *Planta*, *149*(1), 78-90.

Farquhar, G. D., O'Leary, M. H., & Berry, J. A. (1982). On the relationship between carbon isotope discrimination and the intercellular carbon dioxide concentration in leaves. *Functional Plant Biology*, *9*(2), 121-137.

Fletcher, W. J., Müller, U. C., Koutsodendris, A., Christanis, K., & Pross, J. (2013). A centennial-scale record of vegetation and climate variability from 312 to 240 ka (Marine Isotope Stages 9c–a, 8 and 7e) from Tenaghi Philippon, NE Greece. *Quaternary Science Reviews*, *78*, 108-125.

Francke, A., Wagner, B., Just, J., Leicher, N., Gromig, R., Baumgarten, H., ... & Leng, M. J. (2016). Sedimentological processes and environmental variability at Lake Ohrid (Macedonia, Albania) between 637 ka and the present.

Grimm, E. C. (1987). CONISS: a FORTRAN 77 program for stratigraphically constrained cluster analysis by the method of incremental sum of squares. *Computers & geosciences*, *13*(1), 13-35.

Hare, V. J., Loftus, E., Jeffrey, A., & Ramsey, C. B. (2018). Atmospheric CO 2 effect on stable carbon isotope composition of terrestrial fossil archives. *Nature communications*, *9*(1), 252.

Hammer, Ø., Harper, D. A., & Ryan, P. D. (2001). PAST: paleontological statistics software package for education and data analysis. *Palaeontologia electronica*, *4*(1), 9.

Hjelmroos, M., & Franzen, L. G. (1994). Implications of recent long-distance pollen transport events for the interpretation of fossil pollen records in Fennoscandia. *Review of Palaeobotany and Palynology*, *82*(1-2), 175-189.

Hoffmann, N., Reicherter, K., Grützner, C., Hürtgen, J., Rudersdorf, A., Viehberg, F., & Wessels, M. (2012). Quaternary coastline evolution of Lake Ohrid (Macedonia/Albania). *Open Geosciences*, *4*(1), 94-110.

Hopkins, W. G. & Hüner. N. P. A. (2009). Introduction to Plant Physiology, 4th ed. John Wiley & Sons, Inc.

Juggins, S. (2003). C2 User guide. *Software for ecological and palaeoecological data analysis and visualisation. University of Newcastle, Newcastle upon Tyne*, *69*.

Koehne, E. (1893). Deutsche Dendrologie. Stuttgart: Ferdinand Enke.

Köhler, P., Fischer, H., & Schmitt, J. (2010). Atmospheric δ13CO2 and its relation to pCO2 and deep ocean δ13C during the late Pleistocene. *Paleoceanography and Paleoclimatology*, *25*(1).

Kohn, M. J. (2010). Carbon isotope compositions of terrestrial C3 plants as indicators of (paleo) ecology and (paleo) climate. *Proceedings of the National Academy of Sciences*, *107*(46), 19691-19695.

Konijnendijk, T. Y. M., Ziegler, M., & Lourens, L. J. (2015). On the timing and forcing mechanisms of late Pleistocene glacial terminations: insights from a new high-resolution benthic stable oxygen isotope record of the eastern Mediterranean. *Quaternary Science Reviews*, *129*, 308-320.

Kousis, I., Koutsodendris, A., Peyron, O., Leicher, N., Francke, A., Wagner, B., ... & Pross, J. (2018). Centennial-scale vegetation dynamics and climate variability in SE Europe during Marine Isotope Stage 11 based on a pollen record from Lake Ohrid. *Quaternary Science Reviews*, *190*, 20-38.

Lacey, J. H., Leng, M. J., Francke, A., Sloane, H. J., Milodowski, A., Vogel, H., ... & Wagner, B. (2016). Northern Mediterranean climate since the Middle Pleistocene: a 637 ka stable isotope record from Lake Ohrid (Albania/Macedonia).

LaDeau, S. L., & Clark, J. S. (2006). Pollen production by Pinus taeda growing in elevated atmospheric CO2. *Functional Ecology*, *20*(3), 541-547.

Lambert, F., Bigler, M., Steffensen, J. P., Hutterli, M., & Fischer, H. (2012). Centennial mineral dust variability in high-resolution ice core data from Dome C, Antarctica. *Climate of the Past*, *8*(2), 609-623.

Lisiecki, L. E., & Raymo, M. E. (2005). A Pliocene-Pleistocene stack of 57 globally distributed benthic δ18O records. *Paleoceanography*, *20*(1).

Lindhorst, K., Krastel, S., Reicherter, K., Stipp, M., Wagner, B., & Schwenk, T. (2015). Sedimentary and tectonic evolution of Lake Ohrid (Macedonia/Albania). *Basin Research*, *27*(1), 84-101.

Litt, T., Pickarski, N., Heumann, G., Stockhecke, M., & Tzedakis, P. C. (2014). A 600,000 year long continental pollen record from Lake Van, eastern Anatolia (Turkey). *Quaternary Science Reviews*, *104*, 30-41.

Loulergue, L., Schilt, A., Spahni, R., Masson-Delmotte, V., Blunier, T., Lemieux, B., ... & Chappellaz, J. (2008). Orbital and millennial-scale features of atmospheric CH 4 over the past 800,000 years. *Nature*, *453*(7193), 383.

Loutre, M. F., & Berger, A. (2000). Future climatic changes: Are we entering an exceptionally long interglacial?. *Climatic Change*, *46*(1-2), 61-90.

Lundberg, J., & McFarlane, D. A. (2007). Pleistocene depositional history in a periglacial terrane: A 500 ky record from Kents Cavern, Devon, United Kingdom. *Geosphere*, *3*(4), 199-219.

Lüthi, D., Le Floch, M., Bereiter, B., Blunier, T., Barnola, J. M., Siegenthaler, U., ... & Stocker, T. F. (2008). High-resolution carbon dioxide concentration record 650,000–800,000 years before present. *Nature*, *453*(7193), 379.

Magri, D., Di Rita, F., Aranbarri, J., Fletcher, W., & González-Sampériz, P. (2017). Quaternary disappearance of tree taxa from Southern Europe: Timing and trends. *Quaternary Science Reviews*, *163*, 23-55.

Martrat, B., Grimalt, J. O., Shackleton, N. J., de Abreu, L., Hutterli, M. A., & Stocker, T. F. (2007). Four climate cycles of recurring deep and surface water destabilizations on the Iberian margin. *Science*, *317*(5837), 502-507.

Matevski, V., Èarni, A., Avramoski, O., Juvan, N., Kostadinovski, M., Košir, P., ... & Šilc, U. (2011). *Forest Vegetation of Galièica Mountain Range in Macedonia*. Založba ZRC.

Matzinger, A., Spirkovski, Z., Patceva, S., & Wüest, A. (2006). Sensitivity of ancient Lake Ohrid to local anthropogenic impacts and global warming. *Journal of Great Lakes Research*, *32*(1), 158-179.

McManus, J. F., Oppo, D. W., & Cullen, J. L. (1999). A 0.5-million-year record of millennial-scale climate variability in the North Atlantic. *science*, *283*(5404), 971-975.

Médail, F., & Diadema, K. (2009). Glacial refugia influence plant diversity patterns in the Mediterranean Basin. *Journal of biogeography*, *36*(7), 1333-1345.

Meinzer, F. C., Johnson, D. M., Lachenbruch, B., McCulloh, K. A., & Woodruff, D. R. (2009). Xylem hydraulic safety margins in woody plants: coordination of stomatal control of xylem tension with hydraulic capacitance. *Functional Ecology*, *23*(5), 922-930.

Milankovitch, M. K. (1941). Kanon der Erdbestrahlung und seine Anwendung auf das Eiszeitenproblem. *Royal Serbian Academy Special Publication*, *133*, 1-633.

Moore, P. D., Webb, J. A., & Collison, M. E. (1991). *Pollen analysis*. Blackwell scientific publications.

Moran, J. J., Newburn, M. K., Alexander, M. L., Sams, R. L., Kelly, J. F., & Kreuzer, H. W. (2011). Laser ablation isotope ratio mass spectrometry for enhanced sensitivity and spatial resolution in stable isotope analysis. *Rapid Communications in Mass Spectrometry*, *25*(9), 1282-1290.

Nelson, D. M. (2012). Carbon isotopic composition of Ambrosia and Artemisia pollen: assessment of a C3-plant paleophysiological indicator. *New Phytologist*, *195*(4), 787-793.

Obreht, I., Zeeden, C., Hambach, U., Veres, D., Marković, S. B., Bösken, J., ... & Lehmkuhl, F. (2016). Tracing the influence of Mediterranean climate on Southeastern Europe during the past 350,000 years. *Scientific reports*, *6*, 36334.

Parrenin, F., Barnola, J. M., Beer, J., Blunier, T., Castellano, E., Chappellaz, J., ... & Kawamura, K. (2007). The EDC3 chronology for the EPICA Dome C ice core. *Climate of the Past*, *3*, 485-497.

Petit, J. R., Jouzel, J., Raynaud, D., Barkov, N. I., Barnola, J. M., Basile, I., ... & Delmotte, M. (1999). Climate and atmospheric history of the past 420,000 years from the Vostok ice core, Antarctica. *Nature*, *399*(6735), 429.

Popovska, C., & Bonacci, O. (2007). Basic data on the hydrology of Lakes Ohrid and Prespa. *Hydrological Processes: An International Journal*, *21*(5), 658-664.

Prentice, I. C., Dong, N., Gleason, S. M., Maire, V., & Wright, I. J. (2014). Balancing the costs of carbon gain and water transport: testing a new theoretical framework for plant functional ecology. *Ecology letters*, *17*(1), 82-91.

Pross, J., Koutsodendris, A., Christanis, K., Fischer, T., Fletcher, W. J., Hardiman, M., ... & Müller, U. C. (2015). The 1.35-Ma-long terrestrial climate archive of Tenaghi Philippon, northeastern Greece: Evolution, exploration, and perspectives for future research. *Newsletters on Stratigraphy*, *48*(3), 253-276.

Railsback, L. B., Gibbard, P. L., Head, M. J., Voarintsoa, N. R. G., & Toucanne, S. (2015). An optimized scheme of lettered marine isotope substages for the last 1.0 million

years, and the climatostratigraphic nature of isotope stages and substages. *Quaternary Science Reviews*, *111*, 94-106.

Regattieri, E., Zanchetta, G., Isola, I., Bajo, P., Perchiazzi, N., Drysdale, R. N., ... & Wagner, B. (2018). A MIS 9/MIS 8 speleothem record of hydrological variability from Macedonia (FYROM). *Global and planetary change*, *162*, 39-52.

Reille, M., Beaulieu, J. L. D., Svobodova, H., Andrieu-Ponel, V., & Goeury, C. (2000). Pollen analytical biostratigraphy of the last five climatic cycles from a long continental sequence from the Velay region (Massif Central, France). *Journal of Quaternary Science: Published for the Quaternary Research Association*, *15*(7), 665-685.

Ribolini, A., Isola, I., Zanchetta, G., Bini, M., & Sulpizio, R. (2011). Glacial features on the Galicica Mountains, Macedonia: preliminary report. *Geogr. Fis. Din. Quat*, *34*, 247-255.

Rohling, E. J., Grant, K., Bolshaw, M., Roberts, A. P., Siddall, M., Hemleben, C., & Kucera, M. (2009). Antarctic temperature and global sea level closely coupled over the past five glacial cycles. *Nature Geoscience*, *2*(7), 500.

van Roij, L., Sluijs, A., Laks, J. J., & Reichart, G. J. (2017). Stable carbon isotope analyses of nanogram quantities of particulate organic carbon (pollen) with laser ablation nano combustion gas chromatography/isotope ratio mass spectrometry. *Rapid Communications in Mass Spectrometry*, *31*(1), 47-58.

Roucoux, K. H., Tzedakis, P. C., De Abreu, L., & Shackleton, N. J. (2006). Climate and vegetation changes 180,000 to 345,000 years ago recorded in a deep-sea core off Portugal. *Earth and Planetary Science Letters*, *249*(3-4), 307-325.

Ruddiman, W. F. (2007). The early anthropogenic hypothesis: Challenges and responses. Reviews of Geophysics, 45(4).

Saaroni, H., Bitan, A., Alpert, P., & Ziv, B. (1996). Continental polar outbreaks into the Levant and eastern Mediterranean. *International Journal of Climatology*, *16*(10), 1175-1191.

Sadori, L., Koutsodendris, A., Panagiotopoulos, K., Masi, A., Bertini, A., Combourieu-Nebout, N., ... & Mercuri, A. M. (2016). Pollen-based paleoenvironmental and paleoclimatic change at Lake Ohrid (south-eastern Europe) during the past 500 ka.

San-Miguel-Ayanz, J., de Rigo, D., Caudullo, G., Durrant, T. H., Mauri, A., Tinner, W., ... & Enescu, C. M. (2016). European atlas of forest tree species.

Saurer, M., Siegwolf, R. T., & Schweingruber, F. H. (2004). Carbon isotope discrimination indicates improving water-use efficiency of trees in northern Eurasia over the last 100 years. *Global Change Biology*, *10*(12), 2109-2120.

Seppä, H. (2007). Pollen analysis, principles. *Encyclopedia of Quaternary Science*, *3*, 2486-2497.

Sinopoli, G., Masi, A., Regattieri, E., Wagner, B., Francke, A., Peyron, O., & Sadori, L. (2018). Palynology of the Last Interglacial Complex at Lake Ohrid: palaeoenvironmental and palaeoclimatic inferences. *Quaternary Science Reviews*, *180*, 177-192.

Smit, A. (1973). A scanning electron microscopical study of the pollen morphology in the genus Quercus. *Acta botanica neerlandica*, *22*(6), 655-665.

Stankovic, S., 1960. The Balkan Lake Ohrid and its Living World, Monogr. Biol.IX, Uitgeverij Dr. W. Junk, Den Haag, the Netherlands.

Stockmarr, J. A. (1971). Tabletes with spores used in absolute pollen analysis. *Pollen spores*, *13*, 615-621.

Tzedakis, P. C. (1994). Vegetation change through glacial—interglacial cycles: a long pollen sequence perspective. *Philosophical Transactions of the Royal Society of London. Series B: Biological Sciences*, *345*(1314), 403-432.

Tzedakis, P. C., Andrieu, V., De Beaulieu, J. L., Crowhurst, S. D., Follieri, M., Hooghiemstra, H., ... & Wijmstra, T. A. (1997). Comparison of terrestrial and marine records of changing climate of the last 500,000 years. *Earth and Planetary Science Letters*, *150*(1-2), 171-176.

Tzedakis, P. C., Andrieu, V., De Beaulieu, J. L., Birks, H. J. B., Crowhurst, S., Follieri, M., ... & Shackleton, N. J. (2001). Establishing a terrestrial chronological framework as a basis for biostratigraphical comparisons. *Quaternary Science Reviews*, *20*(16-17), 1583-1592.

Tzedakis, P. C., Lawson, I. T., Frogley, M. R., Hewitt, G. M., & Preece, R. C. (2002). Buffered tree population changes in a Quaternary refugium: evolutionary implications. *science*, *297*(5589), 2044-2047.

Tzedakis, P. C., Roucoux, K. H., De Abreu, L., & Shackleton, N. J. (2004). The duration of forest stages in southern Europe and interglacial climate variability. *Science*, *306*(5705), 2231-2235.

Tzedakis, P. C., Hooghiemstra, H., & Pälike, H. (2006). The last 1.35 million years at Tenaghi Philippon: revised chronostratigraphy and long-term vegetation trends. *Quaternary Science Reviews*, *25*(23-24), 3416-3430.

Tzedakis, P. C., Raynaud, D., McManus, J. F., Berger, A., Brovkin, V., & Kiefer, T. (2009). Interglacial diversity. *Nature Geoscience*, *2*(11), 751.

Wagner, B., Wilke, T., Krastel, S., Zanchetta, G., Sulpizio, R., Reicherter, K., ... & Francke, A. (2014). The SCOPSCO drilling project recovers more than 1.2 million years of history from Lake Ohrid.

Wagner, B., Wilke, T., Francke, A., Albrecht, C., Baumgarten, H., Bertini, A., ... & Donders, T. H. (2017). The environmental and evolutionary history of Lake Ohrid (FYROM/Albania): interim results from the SCOPSCO deep drilling project.

Wagner et al., accepted.

Watzin, M. C., Puka, V., & Naumoski, T. B. (Eds.). (2002). *Lake Ohrid and its watershed: state of the environment report*. Hydrobiological Institute.

Wijmstra, T. A. (1969). Palynology of the first 30 metres of a 120 m deep section in northern Greece. *Acta botanica neerlandica*, *18*(4), 511-527.

Xoplaki, E., González-Rouco, J. F., Luterbacher, J., & Wanner, H. (2003). Mediterranean summer air temperature variability and its connection to the large-scale atmospheric circulation and SSTs. *Climate dynamics*, *20*(7-8), 723-739.

Ziska, L. H., & Caulfield, F. A. (2000). Rising CO2 and pollen production of common ragweed (Ambrosia artemisiifolia L.), a known allergy-inducing species: implications for public health. *Functional Plant Biology*, *27*(10), 893-898.

Appendix 1: Pictures of selected pollen taxa discussed in the text. These are taxa that need extra elaboration on their identification, since most of them are extinct taxa and misinterpretation can lead to false conclusions. Photo A, B and H are taken with 40x magnification, the other photos have 63x magnification. A, B, C, *Carya*, 20-30 µm. D, E, *Pterocarya*, 35µm, F, *Pinus* haploxylon, 60 µm, G, *Pinus* diploxylon, 60 µm, H, small *Abies*, 60 µm (not discussed in the text), I, *Zelkova*, 20-30 µm, J, *Ulmus*, 20-30 µm.

Appendix 2: Samples used in this study, partially counted in this study and partially by Sadori et al., (2016).

Vial	Mean Mcd	Age (ka)	Counted by	Vial	Mean mcd	Age (ka)	Counted by
801	129.06	297.714	Sadori	893	143.79	330.462	Sadori
803	129.39	298.297	This study	895	144.11	331.296	This study
805	129.71	298.861	Sadori	897	144.43	332.14	Sadori
807	130.03	299.423	This study	899	144.75	333.045	This study
809	130.35	300.036	Sadori	901	145.07	333.953	Sadori
811	130.67	300.677	This study	903	145.39	334.881	This study
813	130.99	301.312	Sadori	905	145.71	335.8	Sadori
815	131.31	301.95	This study	907	146.03	336.674	This study
817	131.63	302.555	Sadori	909	146.35	337.545	Sadori
819	131.95	303.161	This study	911	146.67	338.412	This study
821	132.28	303.792	Sadori	913	146.99	339.291	Sadori
823	132.59	304.392	This study	915	147.31	340.409	This study
825	132.91	305.01	Sadori	917	147.63	341.587	Sadori
827	133.23	305.654	This study	919	147.95	342.759	This study
829	133.55	306.299	Sadori	921	148.27	343.928	Sadori
831	133.87	306.938	This study	923	148.59	344.932	This study
833	134.19	307.565	Sadori	925	148.91	345.882	Sadori
835	134.51	308.179	This study	927	149.23	346.832	This study
837	134.83	308.798	Sadori	929	149.55	347.78	Sadori
839	135.15	309.401	This study	931	149.87	348.716	This study
841	135.47	310.003	Sadori	933	150.19	349.647	Sadori
843	135.79	310.587	This study	935	150.51	350.591	This study
845	136.12	311.19	Sadori	937	150.83	351.527	Sadori
847	136.43	311.756	This study	939	151.15	352.485	This study
849	136.75	312.344	Sadori	941	151.47	353.452	Sadori
851	137.07	312.962	This study	943	151.79	354.423	This study
853	137.39	313.592	Sadori	945	152.11	355.389	Sadori
855	137.71	314.223	This study	947	152.43	356.402	This study
857	138.03	314.843	Sadori	949	152.75	357.459	Sadori
859	138.35	315.482	This study	951	153.07	358.523	This study
861	138.67	316.133	Sadori	953	153.39	359.596	Sadori
863	138.99	316.778	This study	955	153.71	360.678	This study
865	139.31	317.421	Sadori	957	154.03	361.761	Sadori
867	139.63	318.061	This study	959	154.35	362.849	This study
869	139.95	318.7	Sadori	961	154.67	363.94	Sadori
871	140.27	319.354	This study	963	154.99	364.983	This study
873	140.59	320.048	Sadori	965	155.31	366.008	Sadori
875	140.91	321.09	This study	967	155.63	367.017	This study
877	141.23	322.127	Sadori	969	155.95	368.039	Sadori
879	141.55	323.128	This study	971	156.43	368.995	This study
881	141.87	324.197	Sadori	973	156.59	369.873	Sadori
883	142.19	325.336	This study	977	157.23	371.635	Sadori
885	142.51	326.485	Sadori	981	157.87	374.041	Sadori
887	142.83	327.634	This study	985	158.51	376.806	Sadori
889	143.15	328.787	Sadori	989	159.15	379.774	Sadori
891	143.47	329.621	This study				

Appendix 3: AP%, AP-*Pinus*% and pollen influx.

Age (ka)	AP %	AP-*Pinus* %	Influx (grains /cm2/year)	Age (ka)	AP %	AP-*Pinus* %	Influx(grains /cm2/year)
297.714	85.04902	54.8148	7481	330.462	94.83283	90.3409	44246
298.297	70.84691	33.209	6962	331.296	91.21813	85.0242	61599
298.861	98.02632	83.5616	7532	332.14	68.89952	64.8649	60108
299.423	90.61224	62.6016	20892	333.045	87.96499	84.9315	118059
300.036	78.01932	43.125	7481	333.953	57.22222	50	20924
300.677	60.22305	20.7407	4197	334.881	52.95567	34.3643	11575
301.312	96.52087	7.89474	Outlier	335.8	42.38683	23.0769	10810
301.95	79.46809	37.9421	9641	336.674	49.1453	33.5196	9322
302.555	84.01535	32.4324	6081	337.545	46.5	32.7044	11315
303.161	88.68661	66.0156	34972	338.412	49.58678	37.1134	6044
303.792	93.42949	71.5278	23233	339.291	45.45455	32	3396
304.392	90	71.2062	26038	340.409	45.88608	39.7887	4736
305.01	92.59259	62.069	8659	341.587	52.10843	37.4016	2066
305.654	78.17204	25.9124	5735	342.759	66.99029	51.2545	4657
306.299	91.43969	68.7943	13772	343.928	55.89888	33.1915	962
306.938	90.89848	72.8223	25675	344.932	56.22407	27.2414	2101
307.565	87.69634	66.4286	15247	345.882	46.59864	19.898	678
308.179	89.1933	74.1818	30147	346.832	50.42735	20.5479	1160
308.798	89.44954	73.0994	30410	347.78	71.55425	33.1034	1054
309.401	87.83455	63.2353	33082	348.716	72.19512	38.0435	2172
310.003	74.8	24.7012	4042	349.647	79.70205	44.9495	1625
310.587	90.51383	73.4317	27319	350.591	78.19225	46.6667	2124
311.19	87.84119	68.5897	23659	351.527	84.21829	48.5577	2004
311.756	87.39496	69.1781	28906	352.485	82.55208	52.3132	4300
312.344	86.24079	71.5736	25079	353.452	71.29456	34.3348	1123
312.962	81.31579	73.9927	55621	354.423	80.47493	47.331	3923
313.592	86.41618	81.8533	38700	355.389	60.67146	27.1111	1151
314.223	82.83582	75.6184	50091	356.402	85.99382	51.773	5275
314.843	90.28926	83.6806	45307	357.459	83.83234	61.244	3215
315.482	85.65815	80.0546	62052	358.523	49.88764	23.6301	1386
316.133	85.52632	79.4007	34446	359.596	59.49721	38.2979	1672
316.778	89.20863	85.4369	104451	360.678	56.51303	25.1724	1330
317.421	74.50495	63.986	18086	361.761	55.1532	30.6034	740
318.061	90.25845	84.9231	67395	362.849	59.15493	25.0923	1293
318.7	76.84426	45.1456	8645	363.94	63.63636	40.8696	1449
319.354	74.79936	44.3262	10022	364.983	58.74263	23.913	1014
320.048	83.03167	39.5161	6112	366.008	58.65922	34.2222	1193
321.09	83.56688	51.5038	No data	367.017	80.56769	38.6207	2200
322.127	87.83422	66.5441	12266	368.039	49.00901	13.1902	2393
323.128	86.32479	70.9091	18955	368.995	65.76169	19.5035	1965
324.197	89.35644	73.9394	12381	369.873	66.83805	24.1176	1996
325.336	89.45908	79.3478	20362	371.635	70.69971	34.3137	
326.485	88.64198	73.7143	5747	374.041	78.99485	46.5574	
327.634	90.50555	82.3799	28901	376.806	52.51678	11.2853	
328.787	96.44269	91.4557	26694	379.774	60.20942	31.1178	
329.621	92.71845	85.2941	105910				

Appendix 4: Lake Ohrid (North Macedonia/Albania) DEEP core – Pollen percentage diagram of NAP (selected taxa) plotted against age (ka) and depth (m). The algal taxa of botryococcus is also shown here. Pollen zone description is listed in Table 1.

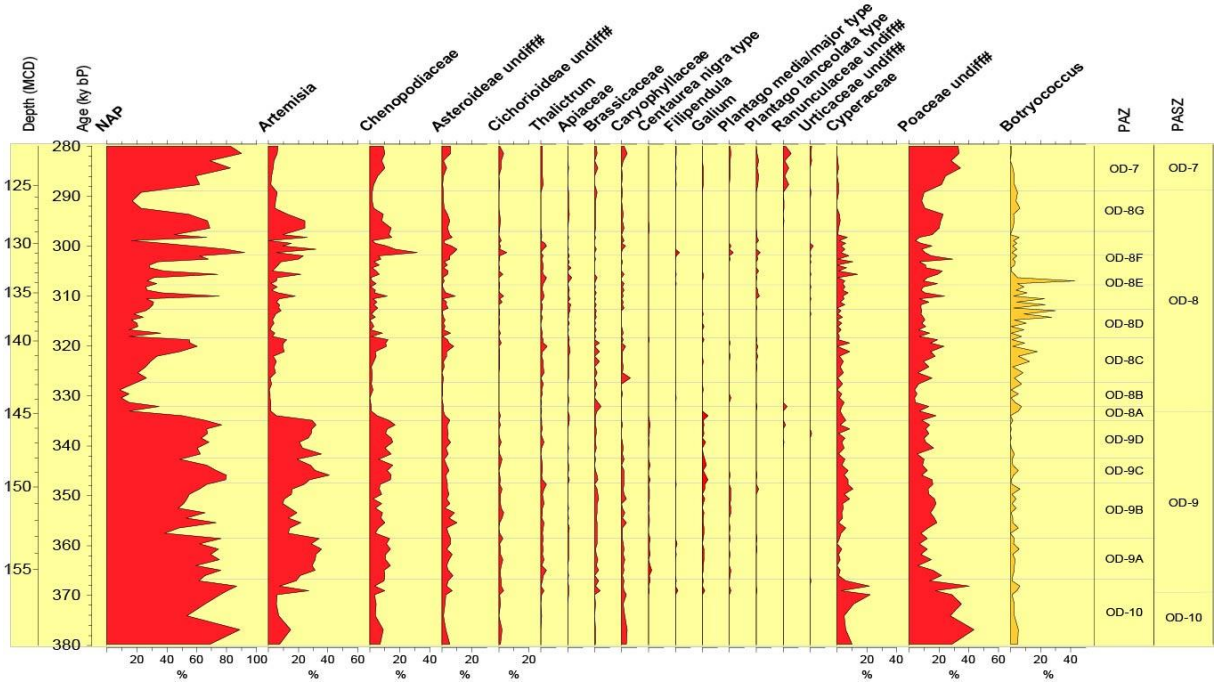

Appendix 5: $\delta^{13}C_{pollen}$ values and their threshold values, against age, per sample. Measurements in red show threshold values of lower than 3.5, which have been excluded for further measurements. For *Abies*, values in green show single pollen with multiple measurements.

Age (ka) 301.95	*Pinus*	Age (ka) 310.587	*Pinus*	Age (ka) 319.354	*Pinus*	Age (ka) 333.045	*Pinus*	Age (ka) 333.953	*Pinus*
$\delta^{13}C$ ‰	threshold	$\delta^{13}C$ ‰	threshold	$\delta^{13}C$ ‰	threshold	$\delta^{13}C$ ‰	threshold	$\delta^{13}C$ ‰	threshold
-27.73	9.71	-29.47	5.35	-26.91	10.29	-27.54	11.54	-26.97	7.16
-27.56	2.16	-26.84	13.53	-24.59	10	-25.11	17.07	-28.03	9
-27.46	1.89	-24.36	9.38	-27.59	7.19	-26.09	11.25	-30.71	3.13
-21.45	1.76	-30.62	5.58	-24.14	8.68	-26.73	15.11	-27.29	7.84
-27.41	6.5	-27.42	7.14	-24.85	7.88	-25.49	12.75	-27.83	9.32
-27.68	4.57	-30.03	10	-28.07	10.65	-28.65	20.26	-28.52	4.24
-26.45	8.75	-26.61	4.44	-24.45	9.51	-27.18	5.37	-28.36	15
-25.49	6.94	-26.12	17.5	-25.41	8.06	-27.61	9.53	-27.86	11.59
-26.36	9.48	-26.94	10.81	-27.22	6.11	-25.70	6	-27.76	5.69
-26.34	2.86	-28.83	9.12	-26.31	6.25	-25.57	14.49	-28.16	11.56
-25.15	3.44	-27.34	6.67	-26.76	10.57	-26.09	8.14	-27.61	11.19
-25.49	2.26	-28.70	8.54	-25.86	15	-27.39	8.95	-29.30	6.61
-27.64	7.45	-28.33	11.79	-24.22	10	-26.74	14.18	-26.80	11.70
-29.72	6.22	-35.00	1.32	-26.09	9.21	-27.22	7.66	-25.63	8.49
-28.23	10.23	-25.89	7.84	-26.12	13.71	-27.62	9.05	-28.37	10.91
-27.81	8.81	-25.56	9.05	-25.69	9.5	-25.54	6	-27.72	9.76
-26.15	12.38	-28.68	6.52	-25.13	8.33	-26.56	11.70	-27.12	5.09
-29.17	4.62	-27.83	7.95	-26.39	7.35	-24.95	9.5	-27.67	8.84
-27.51	7.27	-26.85	10.26	-28.20	6.32	-26.17	6.12	-26.54	8.05
-26.84	7.44	-26.53	3.27	-27.34	9.71	-26.02	4.15	-28.02	8.11
-26.83	6.4	-25.63	4.76	-27.00	15	-25.97	8.68	-28.29	14.88
-26.43	6.67	-30.63	6.92	-28.96	5.14	-27.13	4.71	-25.62	15.61
-25.80	3.54	-28.86	13.25	-26.32	9.71	-26.09	8.78	-27.05	5.33
-25.44	6.90	-29.86	10.25	-27.60	19.39	-24.48	14.75	-27.03	5.22
-29.55	5.38	-25.91	3.54	-26.47	6	-27.82	16.51	-27.86	8.40
-27.92	11.05	-26.74	10	-26.42	15.14	-26.87	11.14	-25.65	11.03
		-28.20	8.21	-27.42	9.49	-26.93	6.73	-28.53	4.5
		-22.38	1.43	-25.87	10	-26.74	11.82	-27.93	6.74
		-26.54	7.69	-25.99	13.71	-26.40	8.54	-26.09	4.88
		-28.81	6.15	-27.63	4.39	-28.06	4.52	-27.62	11.28
				-25.50	9.43	-26.42	5.54	-27.50	11.67
				-28.83	5.41	-27.45	16.67	-26.86	7.5
				-24.80	8.92	-26.77	19.76		
				-28.59	7.71				
				-27.99	6.86				

Appendix 5 (continued)

Age (ka) 346.832 $\delta^{13}C$ ‰	*Pinus* threshold	Age (ka) 360.678 $\delta^{13}C$ ‰	*Pinus* threshold	Age (ka) 310.587 $\delta^{13}C$ ‰	*Abies* threshold	Age (ka) 333.045 $\delta^{13}C$ ‰	*Abies* threshold	Age (ka) 333.045 $\delta^{13}C$ ‰	*Q. robur* threshold
-26.37	9.05	-27.63	10.97	-27.86	19.15	-24.30	19	-30.09	2.09
-28.13	7.22	-28.08	13.10	-27.98	9.25	-24.54	32.4	-27.48	3.24
-27.09	8.37	-27.99	12.96	-26.43	26.82	-25.43	29.23	-26.11	2.93
-25.35	8	-27.08	10.33	-27.19	22.38	-26.96	19.03	-27.11	2.82
-27.13	13.03	-28.02	9.64	-26.42	9.36	-27.03	14.09	-29.89	2.33
-27.82	7.23	-26.50	12.59	-26.21	12.82	-24.32	23.62	-25.85	3.08
-26.74	12.63	-26.47	13.06	-26.18	18.04	-24.25	17.27	-25.57	3.17
-25.75	15.41	-27.56	14.38	-25.44	19.75	-23.34	14.81	-30.97	3.08
-24.20	4	-27.26	12.5	-27.17	25.68	-23.29	11.84	-28.46	2.13
-25.99	8	-29.18	9.14	-26.86	31.39	-25.20	11.96		
-26.84	6.14	-27.06	6.77	-26.06	9.77	-23.59	12.13		
-29.56	2.61	-27.24	7.67	-26.66	15.75	-25.66	22.27		
-25.30	7.69	-29.12	6.58	-28.06	1.58	-25.56	14.56		
-24.19	4.81	-31.21	8.61	-22.79	2.34	-24.91	12.55		
-24.16	5.5	-25.85	14.38	-36.40	1.32	-25.80	12.56		
-32.29	2.75	-26.18	7.10	-26.61	3.67	-24.43	9.30		
-26.37	4.90	-27.31	7.14	-25.19	2.82	-25.76	25.23		
-26.57	15	-26.72	7.88	-26.42	24.57	-24.18	24.44		
-26.63	7.03	-26.32	4.86	-26.93	10.22	-25.01	9.85		
-31.28	2.63	-28.21	7.5	-26.87	19.23	-25.68	18.43		
-29.44	4.36	-26.37	11.56	-27.39	4.63	-25.22	11.02		
-33.26	1.22	-26.93	7.75	-28.94	11.28	-22.52	5.65		
-28.39	3.08	-27.65	9.14	-27.36	12.09	-24.93	5.42		
-29.04	3.89	-27.08	13.53			-23.45	11.36		
-31.12	3.90	-27.79	7.11			-22.20	5.42		
		-27.20	4.41			-25.81	13.96		
		-25.63	13.13			-25.55	20.65		
						-24.76	10.18		
						-24.58	17.66		
						-25.43	6.12		
						-24.35	8.27		
						-24.37	17.92		
						-26.35	8.06		
						-24.98	8.36		
						-22.60	15.31		

Appendix 6: definition of substage boundaries used in this paper, compared with definitions proposed by Railsback et al., (2015), Lacey et al., (2016) and Txedakis et al., (2004). Ages are in kyrs BP. Note that the definitions from site MD01-2443 from the Iberian margin is a marine site, but does agree the most with the proposed definitions in this study. The definition by Railsback et al., (2015) is widely adapted in other papers (Fletcher et al., 2013; Sadori et al., 2016; Regattieri et al., 2018). The studied interval does not cover MIS 9a and the later part of MIS 9b, so the end of MIS 9b is here put at the youngest sample.

Substages	This study	Railsback et al., (2015)	Lacey et al., (2016)	Iberian margin (Tzedakis et al)
9a	-	292-282	293-282	291-276.6
9b	303-297.5 (end of samples)	306-292	308-293	302-291
9c	318.7-303	313-306	318-310	318-302
9d	321.1-318.7	321-313	321-318	324-318
9e	334.9-321.1	336-321	333-321	338-324
10a	347.5-334.9	347.5-336	-	-
10b	358.5-347.5	358.5-347.5	-	-
10c	366.6-358.5	365-358.5	-	-

Appendix 7: Scatterplots of pollen influx against CO_2 concentrations (Bereiter et al., 2015), for *Pinus*, NAP and upland pollen. The pollen influx is the concentration multiplied with the sedimentation rate. Correlations are less highlighted than with the AP-*Pinus* curve, that shows the best match. The Y-axis shows pollen concentration, but pollen influx is shown here.

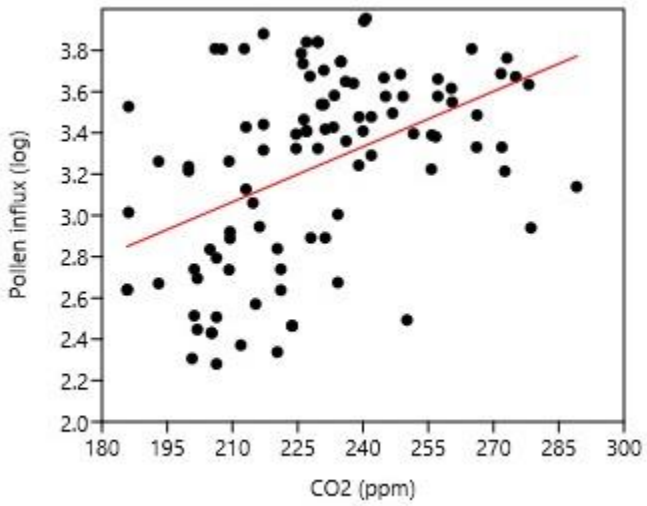

Pinus: r2= 0.20848

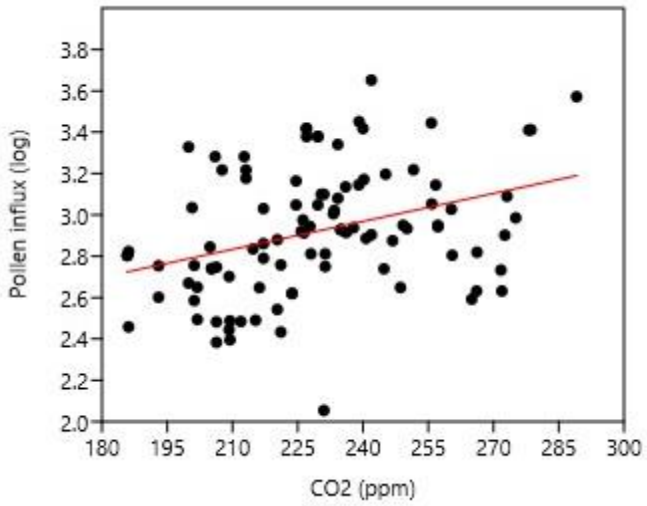

NAP: r2= 0.12048

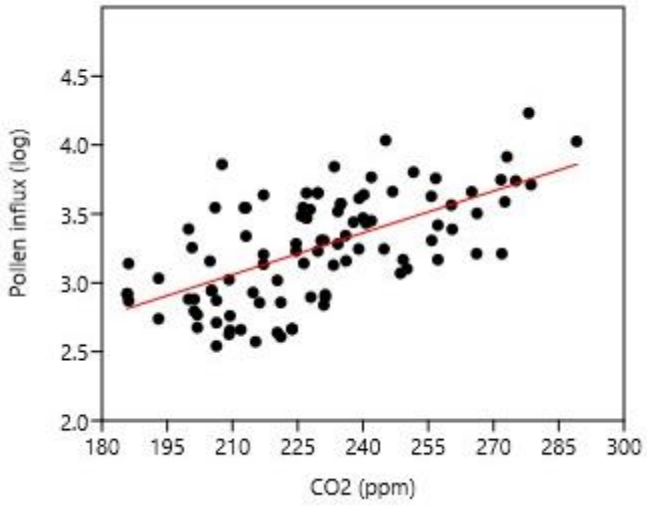

Upland r2= 0.38036

Appendix 8: Histograms of two samples to show threshold changes. Sample 927 (346.832 ka) was selected as it shows large changes by excluding several measurements with each increasing threshold step, while sample 899 (333.045 ka) was selected since it expresses minor changes. Histograms for 899 only start at a threshold level of 4, since no measurements had to be excluded on lower thresholds.

Background 2, number of measurements 25 (927), 33 (899):

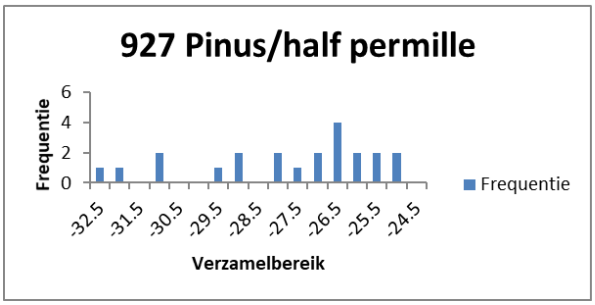

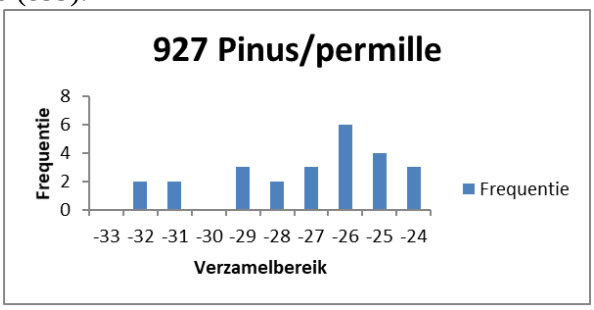

Background 3, number of measurements 22 (927), 33 (899):

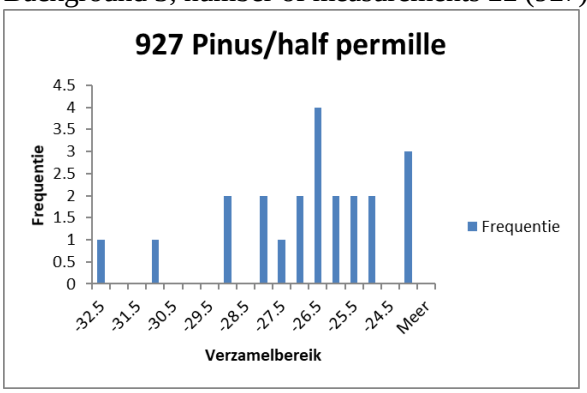

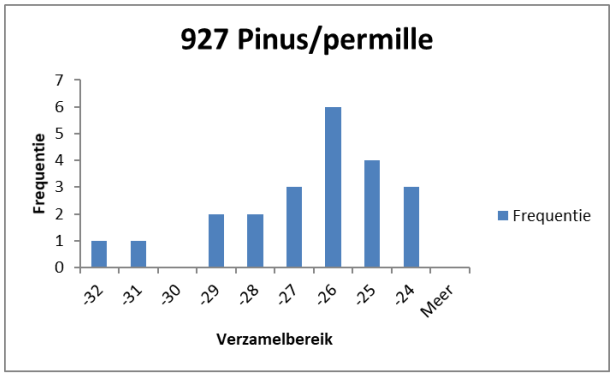

Background 3.5, number of measurements 20 (927), 33 (899):

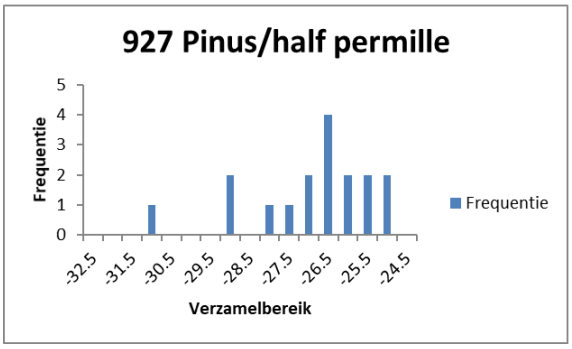

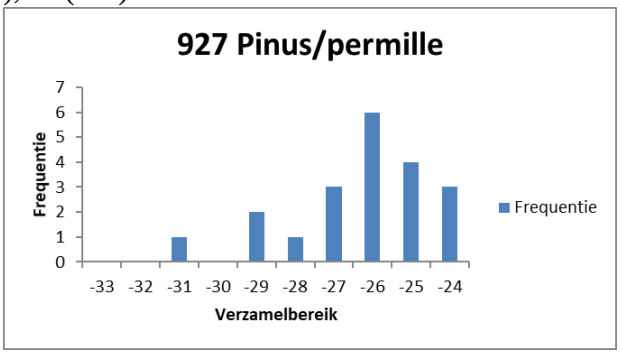

Background 4, number of measurements 17 (927), 33 (899):

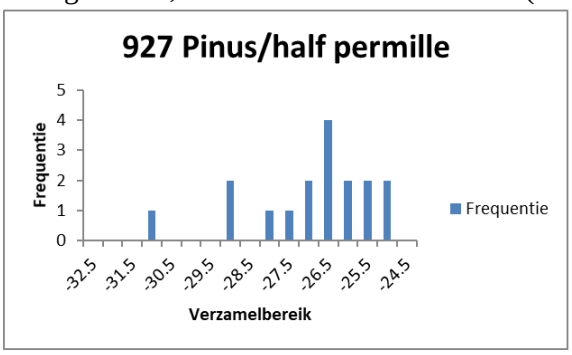

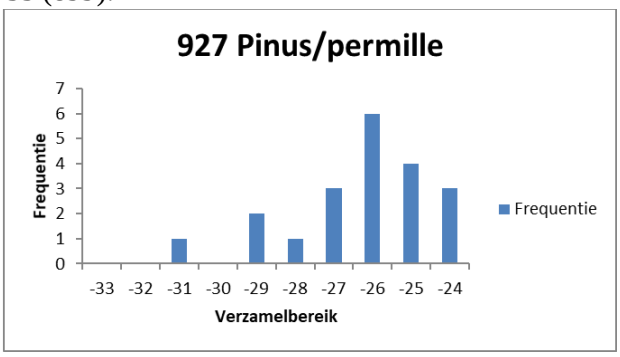

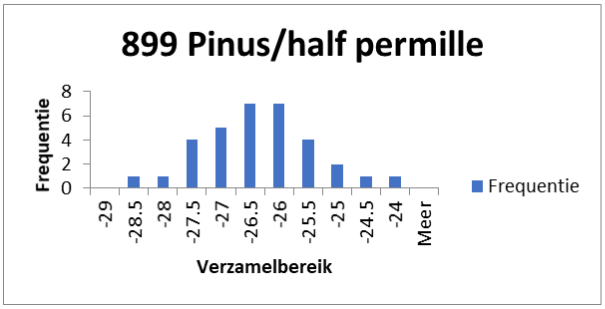

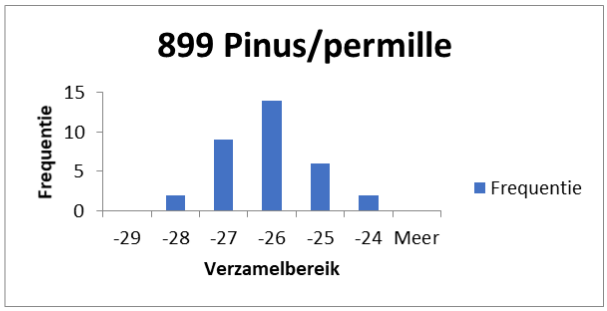

Background 4.5, number of measurements 16 (927), 32 (899):

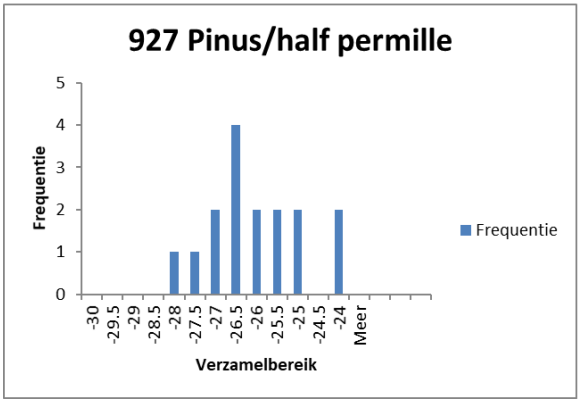

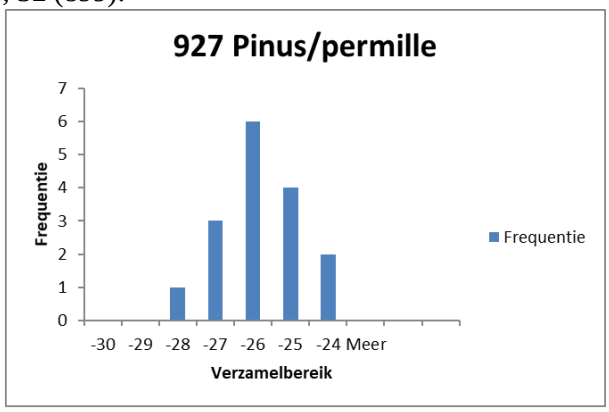

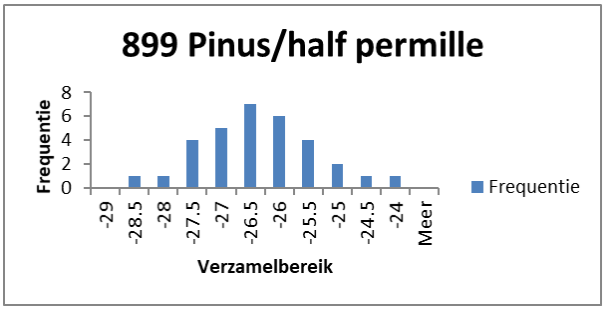

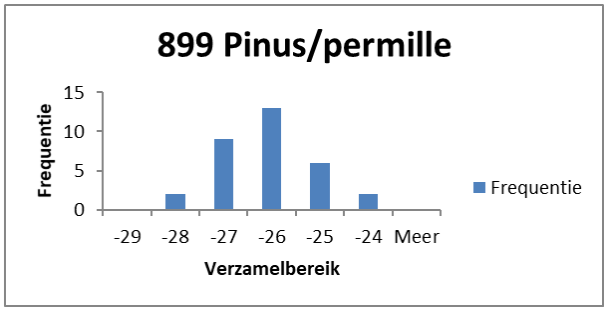

Background 5, number of measurements 14 (927), 30 (899):

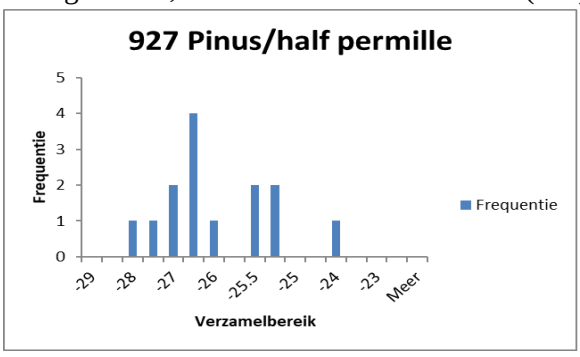

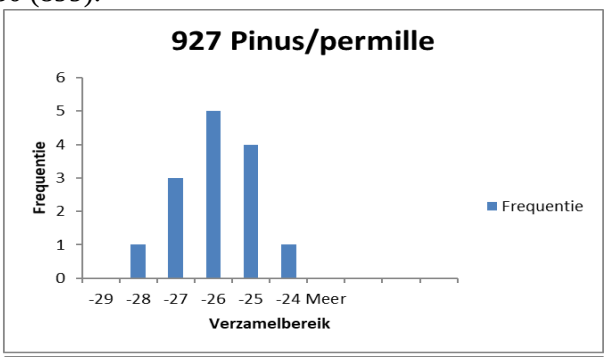

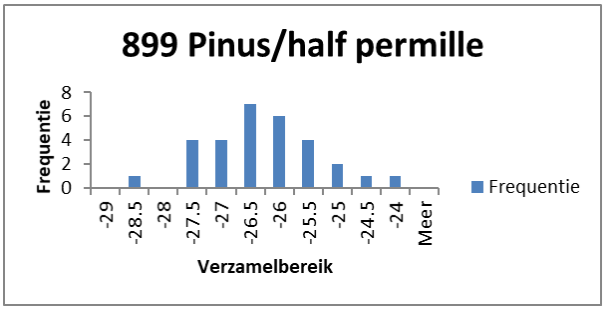

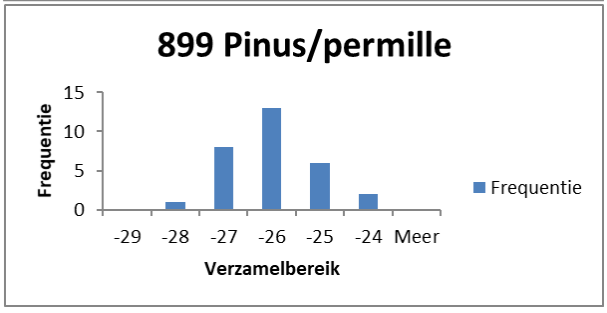

Background 6, number of measurements 13 (927), 26 (899):

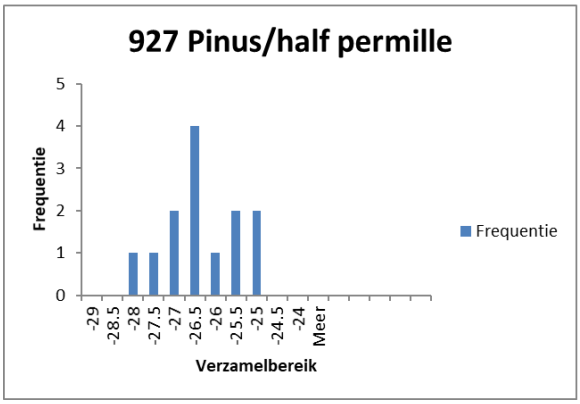

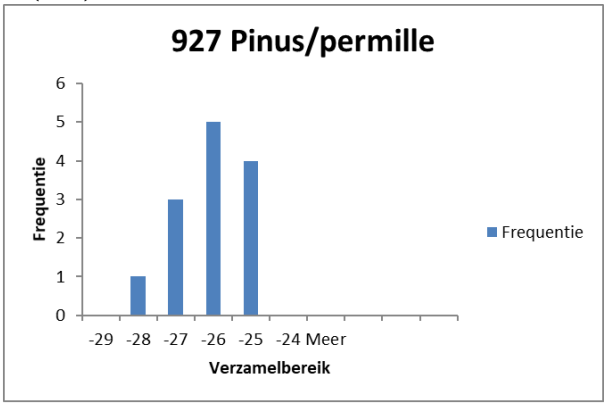

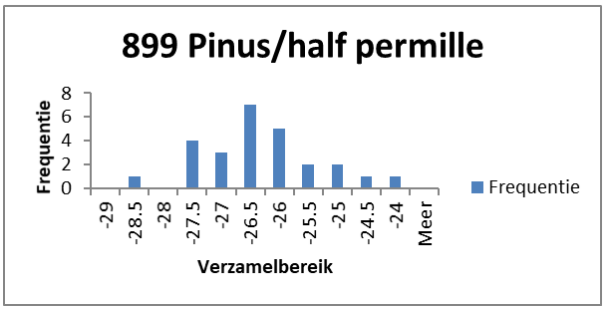

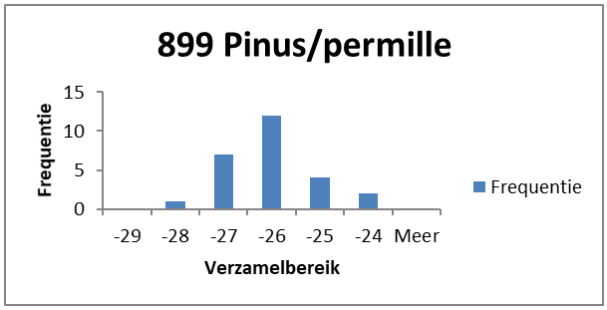

Background 7, number of measurements 12 (927), 24 (899):

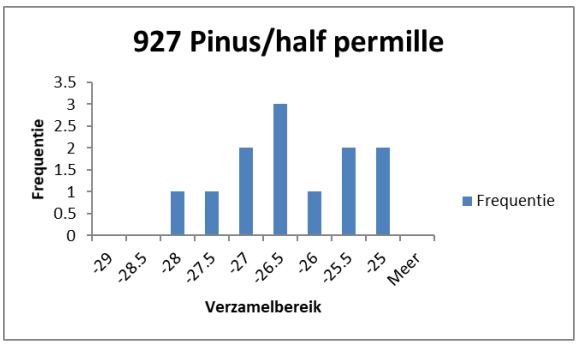

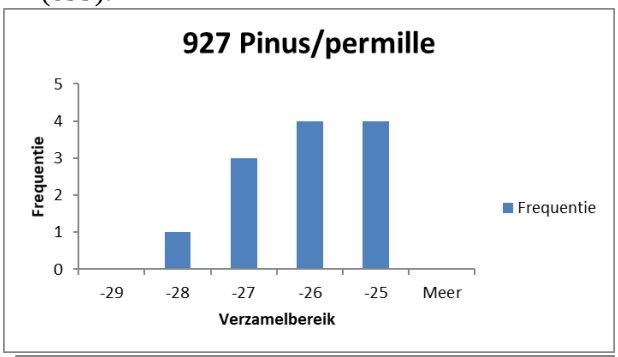

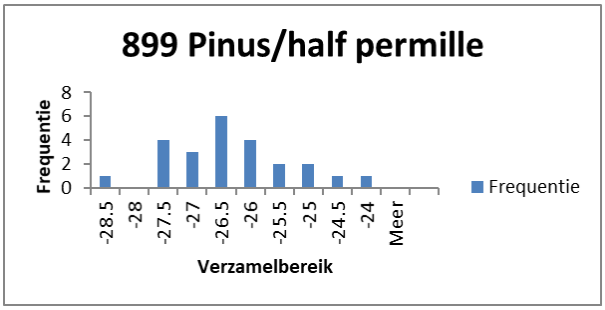

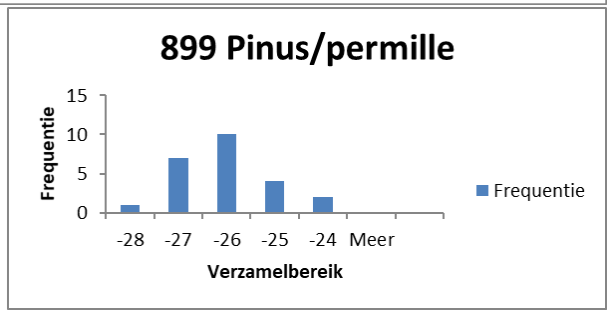

Background 8, number of measurements 6 (927), 23 (899):

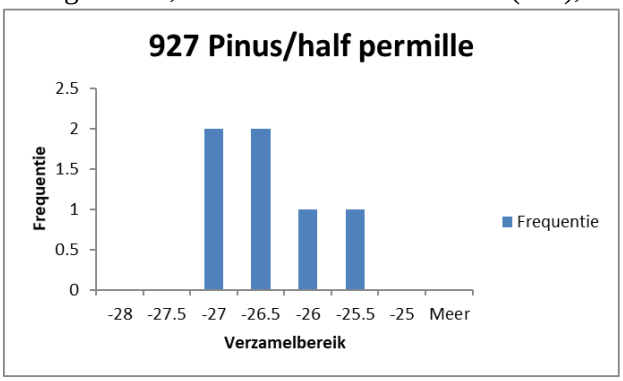

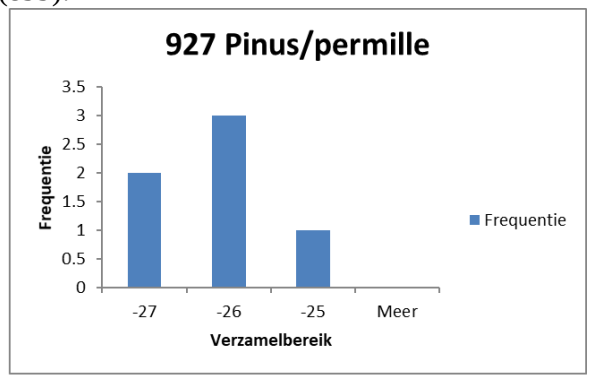

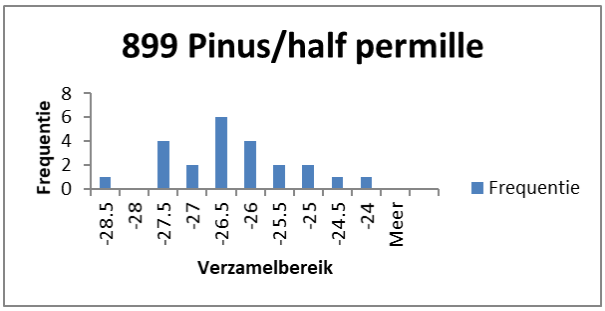

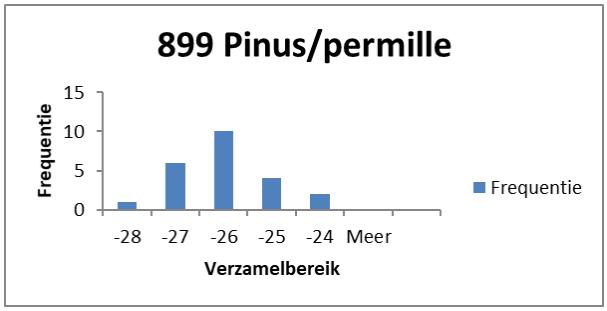

Background 9, number of measurements 5 (927), 18 (899):

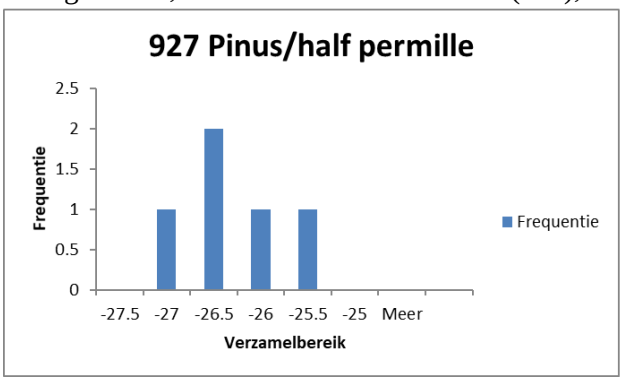

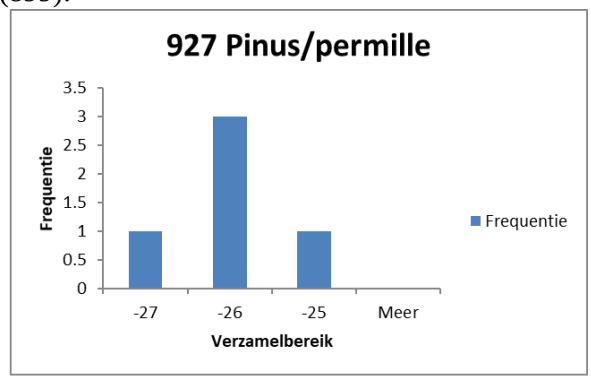

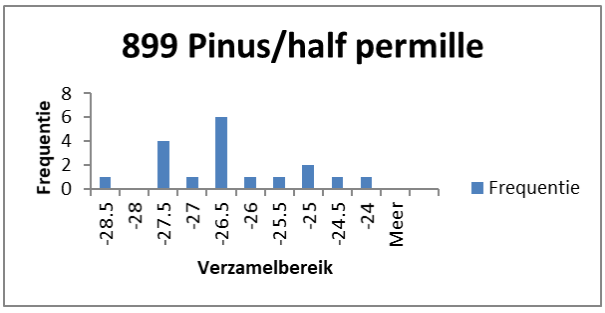

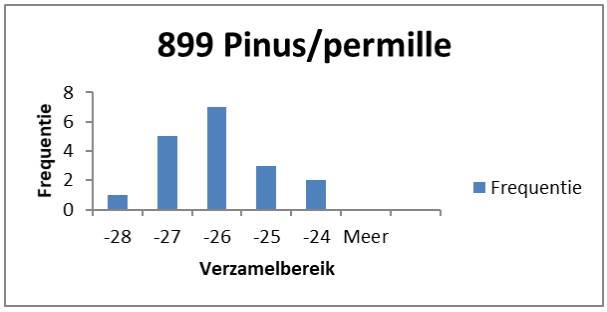

Background 10, number of measurements 4 (927), 15 (899):